Delft University of Technology

Master Thesis

Blast analysis of offshore topside structures

Predicting plastic effects in linear calculations

Author:
Cebrail Aydin

Chairman:
Prof. Dr. A.V. Metrikine

A thesis submitted in partial fulfillment of the requirements for the degree of Master of Science

in

Offshore & Dredging Engineering

December 21, 2015

Graduation committee

Chairman of the graduation committee:

Prof. Dr. A.V. Metrikine, TU Delft

Graduation committee members:

Dr. Ir. P.C.J. Hoogenboom, TU Delft

MSc. N. Bani Shafie, CB&I

Educational institution

Delft University of Technology

Department of Maritime Transport Technology

Faculty of Mechanical, Maritime and Materials Engineering

Address:

Mekelweg 2

2628 CD Delft

The Netherlands

Graduation company

CB&I

Address:

Prinses Beatrixlaan 35

2595 AK The Hague

The Netherlands

DELFT UNIVERSITY OF TECHNOLOGY

Abstract

Faculty of Mechanical, Maritime and Materials Engineering
Offshore & Dredging Engineering

by Cebrail Aydin

One of the most dangerous events that can occur on an offshore topside structure is an explosion. If blast analyses is performed without taking plasticity into account, then it may lead to very conservative design. On the other hand monitoring the weight by optimising the structural design is an important design aspect of such structures.

Considering the time schedule restraints engineers face during the early phases of project, performing advanced non-linear blast analysis is not a practical approach in FEED phase engineering. CB&I, as a leading designer of topsides and processing equipment for offshore oil and gas production, plans to include the effect of advanced blast analysis in the early design phase by including plasticity effect in linear dynamic calculations and define a maximum unity check exceedance ratio which can be proved safe if the plasticity was taken into account.

To this end, a study has been performed of the acceptable unity check exceedance for the preliminary linear dynamic calculations. Furthermore, the influence of the strain rate effect has been investigated.

The acceptable unity check exceedance was analysed in SACS (FEM software package) by comparing the results of the elastic dynamic and plastic dynamic analysis of multiple frame structures. Analytic calculations were performed to verify the results. The influence of the strain rate effect is studied in SACS by using the strain progression over time of a simply supported beam exposed to various blast loads and the corresponding strain rate is determined. This was subsequently used in the constitutive equation of Cowper and Symonds to obtain the dynamic flow stress. The inclusion of the material sensitivity in linear calculations is achieved by comparing the increase of the dynamic flow stress to the static flow stress.

It was found that a generic rule for the exceedance of the unity check was not possible to obtain with the used approach. However, due to the rapid exertion of the blast load a temporary increase of material strength of approximately 20%-27% can be achieved. This can be utilised in blast analysis by increasing the material strength by this percentage, both for linear and non linear dynamic analysis.

Acknowledgements

I would like to take this opportunity to express my gratitude to all the people who guided and helped me completing my thesis.

First of all I would like to thank MSc. N. Bani Shafie for her advice and guidance and all the colleagues from CB&I for their willingness to help.

My deep gratitude goes out to Prof. Dr. A.V. Metrikine for guiding me through the whole process and for his insightful comments.

I would like to extend my sincerest thanks and appreciation to Dr. Ir. P.C.J. Hoogenboom for thinking along with me and providing me with helpful suggestions.

Last but definitely not least, I would like to express my sincere gratitude to my family and classmates for their morale support. Their contribution was undoubtedly of importance to complete my thesis.

Cebrail Aydin
The Hague, December 2015

Contents

List of Figures

List of Tables

Abbreviations

ALS	**A**ccidental **L**imit **S**tates
ASCE	**A**merican **S**ociety of **C**ivil **E**ngineers
CB&I	**C**hicago **B**ridge & **I**ron
CFD	**C**omputanional **F**luid **D**ynamics
DAL	**D**imensioning **A**ccidental **L**oads
EPC	**E**ngineering **P**roduction and **C**onstruction
FEED	**F**ront **E**nd **E**ngineering **D**esign
FEM	**F**inite **E**lement **M**ethod
FPSO	**F**loating **P**roduction **S**torage and **O**ffloading
SACS	**S**tructural **A**nalysis **C**omputer **S**oftware
TNT	**T**ri **N**itro **T**oluene
UC	**U**nity **C**heck

Dedicated to my family

Chapter 1

Introduction

This thesis is not particular based on a project, but the thesis was inspired by the Aasta Hansteen project, where CB&I is contracted for the design of the topside of the spar structure, see figure 1.1a. The notion is to keep the analysis general for topsides in order to use the outcomes of the results and use this knowledge on other projects that differs from a topside on a spar structure. The construction of the hull and topside will be carried out by Hundai Heavy Industries in South Korea. The operator and biggest share holder is Statoil. Aasta Hansteen will be the largest, in terms of diameter and displacement (height of 198 m of which 177 m will be submerged) and the first spar structure with storage for natural gas liquids stored in the hull beneath sea level and where offloading is done by use of a shuttle tanker. The field is located on the Norwegian sea at a water depth of 1300 m, see figure 1.1b.

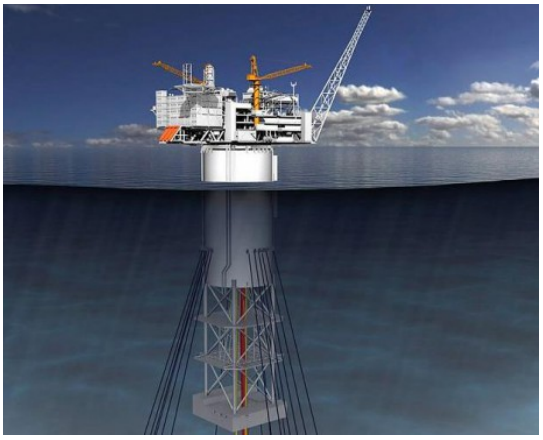

(A) Aasta Hansteen FPSO.

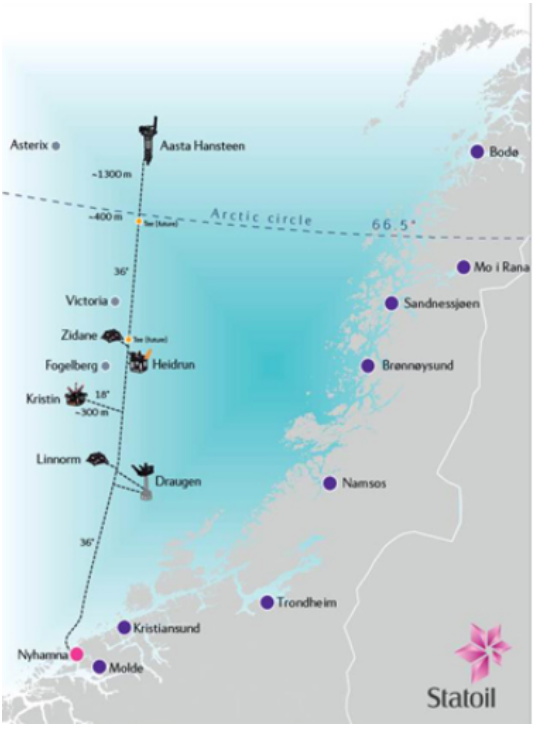

(B) Location of the FPSO.

FIGURE 1.1: [source: www.statoil.com]

1.1 Problem definition

During the early design phase, also known as FEED, of an offshore topside structure a topside blast analyses is performed as part of the ALS analysis. The analysis is performed to demonstrate the feasibility of the chosen structural system and the structural integrity during an explosion. This analysis is mainly performed elastic dynamic, because of it simplicity and the reduction on computational calculation time. The downside of this is that elastic dynamic calculations do not utilise the full strength capacity of the material. In order to keep the UC below one, the structural element is over-designed compared to an analysis which allows plasticity and this leads to increased weight and costs. However ductile materials, such as steel used in the offshore industry have considerable reserve capacity beyond the initial yield stress and this is not taken into account in elastic calculations. Since the engineers know the reserve capacity will lead to smaller structural elements in the later phase of the detail design, also known as EPC they often tolerate, in FEED the UC to be higher than one. The amount of exceedance is not defined and this could be a risk for the later phase in EPC due to the necessity of redesigning the structural element. It is trivial that this could have a significant impact on costs and lead to delay of the project.

It is thus advisable that engineers nowadays should take into account this reserve capacity of steel in the early design phase for blast analysis. This helps to come as close to the final design in terms of dimensioning the primary beams and columns in order to minimize the risk of under dimensioning the structure and without too much over dimensioning the structure.

1.2 Problem statement

Designing topside structures in FEED phase using linear elastic calculations leads to relatively large and heavy structural elements. CB&I intends to incorporate plasticity in linear calculations in order to have more reliable results in the early design phase. Another notion is to make improvement to the design to offer better resistance against the blast loads. This is by means of designing such a structural arrangement in FEED that the structure will have less trouble from the blast load.

The aim of this study is to increase the accuracy of the early design phase regarding blast analysis. The focus is on the primary beam and columns of the topside, because the purpose is to keep the main structure intact after a blast load occurs. A blast analysis is nowadays more demanded in the early design phase as part of the accidental limit state. To meet those demands CB&I is interested in incorporating plasticity in linear calculations and/or have boundaries on exceeding unity checks to minimize the uncertainties in later design phase and increase the reliability of early structural design. The current approach is based on a factor increase of 0.3 found in guideline of ASCE, but CB&I is interested if this factor is justified.

Another issue is improvements for the main structural elements to ensure that the design structure is capable of withstanding the blast load and that the damage on the beam/column is limited in order to retain overall structural strength and stability.

Initially, a progressive collapse analysis seemed to look a good approach to compare the results before and after the explosion damage. The progressive collapse refers to the phenomenon in which the local damage of a primary structural element leads to total or partial structural failure, without any proportionality between the initial and final damage. Some of the potential loads that can lead to progressive collapse are: aircraft impact, design/construction error, fire, explosion, accidental overload and so forth. This analysis could be served to find an acceptable over-dimensioning of the initial beam(s) and/or column(s) that incorporates the loss of a column due to the explosion. However this analysis is often used for buildings consisting of multiple beams and columns, where the effect of removing a column or several ones are analysed. Regarding this thesis the

focus of the analysis is more on the primary beams and columns of topside structures. The topside of a spar like the Aasta Hansteen and the topside modules on an FPSO are supported with fewer, but larger columns and beams. It would be most likely unacceptable that one of this structural element fail completely, since is has less redundancy compared with a building consisting of multiple columns. Besides, this analysis would be too specific regarding the structural arrangement and it would be difficult to use and extend the findings to other structural arrangements.

1.3 Objective

The problem and subject of this thesis converges to the following research questions:

1. *How much excess of unity check is acceptable in preliminary linear calculations?*
2. *What is the influence of strain rate effect?*

1.4 Approach

The approach of the fist objective consist of a linear and non linear analysis of multiple frame structures. The size of the beam and columns were varied and the obtained results were compared. The analysis was performed by the use of SACS software, which is a widely used software in the offshore industry and also by CB&I. A verification of the software with an analytic calculation was also performed. The approach for the second objective was accomplished by using the strain progression in time from SACS for a simple supported beam excited by a blast load for different cases. The strain rates were then used in the constitutive equation of Cowper and Symonds to determine the dynamic flow stress. By doing so the increase was compared to static yield stress and incorporated in linear calculations.

1.5 Thesis structure

The report is structured into the following chapters.

Chapter 1 starts with an introduction to the problem and the objectives of this thesis.

Chapter 2 gives an introduction about the source and development of an explosion on an offshore topside structure and the modelling of the blast load.

Chapter 3 presents the method used to incorporate plasticity in linear calculation and discuss the results of this analysis.

Chapter 4 will present the strain rate effect taking place due to the blast load and discuss the results and implementation of this effect in linear calculations.

Chapter 5 presents the conclusions based on results of the analysis and ends with several recommendations.

Chapter 2

Determining blast load

The blast load is one of the most important parameters to determine whether the structural integrity is sufficient. Unfortunately, this load is also one of the most uncertain parameter, since the blast load depends on multiple factors, such as maximum pressure, rise time and pulse duration. Based on the probabilistic explosion analysis carried out by the third party Lloyd's Register Consulting (also known as Scandpower), the explosion risks have been evaluated and the corresponding blast pressures and associated time durations have been obtained for various locations on the platform. This data is later on used by CB&I as input for further analysis.

As an introduction to blast load analysis, the next section describes the different type of explosions. Furthermore, a general simplification of the explosion load modelling is defined. Finally, an explanation of the blast profile used further on is presented.

2.1 Types of explosion

Explosions can be generally be categorized into two types, detonation and deflagration. Detonation involves a supersonic energy release generating high pressures and temperatures. The expansion of gases after detonation compresses the surrounding air into a pressure wave. This is also known as a shock wave. This happens, because the wave moves faster than the speed of sound in the medium, this is 6900 m/s for TNT. The shock wave is characterized by an abrupt, nearly discontinuous change in pressure, temperature and density of the medium. The wave propagates radially in all directions from the explosion site. When this happens in air, it is called a free air explosion. Close to the surface the waves reflect back to form a half hemisphere. The effect causes almost two times larger pressure than a free air explosion. Figure 2.1 shows the pressure wave expanding outward from the explosive core.

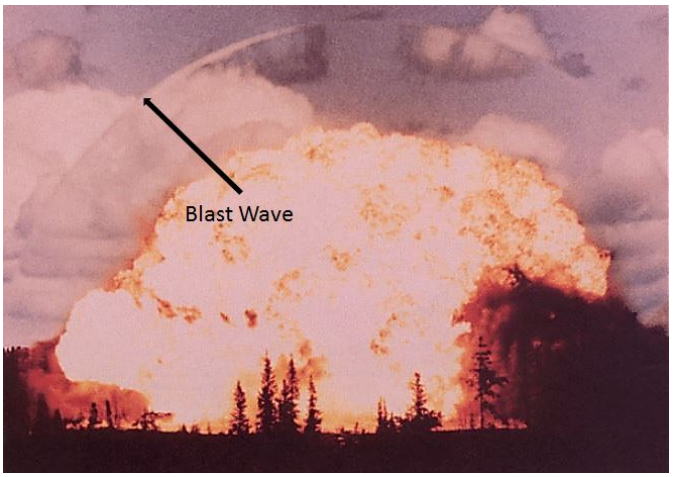

FIGURE 2.1: Expanding blast wave. [13]

In a deflagration, the combustion or reaction wave propagates at a velocity less than the speed of sound through heat transfer, generally less than 100 m/s. The mechanism of combustion propagation is of a flame front that moves forward and each next layer of cold material is heated and ignited by the hot burning material. In essence, the difference between detonation and deflagration is the speed of propagation and the type of propagation (shock wave versus heat transfer). A transition of deflagration into a detonation is possible in some cases. Mainly under geometrical conditions, a subsonic flame may accelerate to supersonic speed. Such a geometrical condition could be a partial confinement and obstacles in the path of the flame that cause turbulent flame eddy currents, hence the transitioning from deflagration to detonation. The mechanism is not fully understood and there is yet no theory which predicts this transition phenomenon. However there are theories that explain and model deflagration and detonation.

The explosion will in this study be assumed as a deflagration, since this is the most probable type of explosion that will occur in an offshore structure, because of the relative slow energy release of oil/gas. Therefore the pressure-time profile will be based on deflagration explosion.

2.2 Probabilistic explosion analysis

A probabilistic explosion analysis serves as a base to determine the blast loads on a structure in offshore application. This analysis is usually performed for the main process area and the weather deck to evaluate the explosion risk and thus the pressure-time profile used in analysis. The following subsections provides an introduction to the method used to determine the blast load on the structure. The procedures and information described

in these subsections are based on the requirements of Norsok Z-013 [1] and performed by Lloyd's Register Consulting in the technical reports of [4] and [16].

2.2.1 Geometry modelling

The modelling of the explosion starts with the geometry of the topside. The geometry model needs to be modelled as realistic as possible. For Aasta Hansteen the model consist of main structures and equipments and some adjustments to make the model suitable for CFD-simulations. The propagation of the flame in case of an explosion will depend upon the physical circumstances i.e. thermodynamic state and the gas composition as well as the surrounding geometry. In order to get realistic results these parameters need to reflect the real situation. The explosion modelling is done before having the definitive model of the topside and in order to compensate this, additional smaller scale cylinder and boxes are added to the geometry model in the early design model to achieve a more realistic level of congestion in the geometry model used in the simulation. It may be required to carry out sensitivity studies on the effect of changing the congestion level for the analysis in the early design phase.

2.2.2 Leak picture

The next step to determine the blast load is by studying the hydrocarbon leaks. This is done by calculating leak frequency using a function of equipment diameter and hole diameter, as well as a number of equipments and locations on the topside specific parameters. The model calculating the leak frequency is based on utilising historical data. The leak frequency is distributed in leak categories determined by the initial leak rates to calculate the accumulated frequency as a function of pressure.

2.2.3 Gas dispersion

Subsequently, several hundred gas dispersion simulations are performed for a large selection of leak rates, locations and wind directions. The number of CFD-simulated scenarios are given by:

$$N = N_a N_{ld} N_{wd} N_{lr} N_{ws} \tag{2.1}$$

Where, N_a is the number of leak locations, N_{ld} the number of leak directions, N_{wd} the number of wind directions, N_{lr} the number of leak rates and N_{ws} the number of wind speeds. The CFD simulated scenarios and the approximated scenarios are used in the probabilistic analysis. Based on this study insight is given into how gas leak will disperse

and expose potential ignition sources. Figure 2.2 shows an example of 100 kg/s gas leak on the mezzanine deck with a 6 m/s wind from the east.

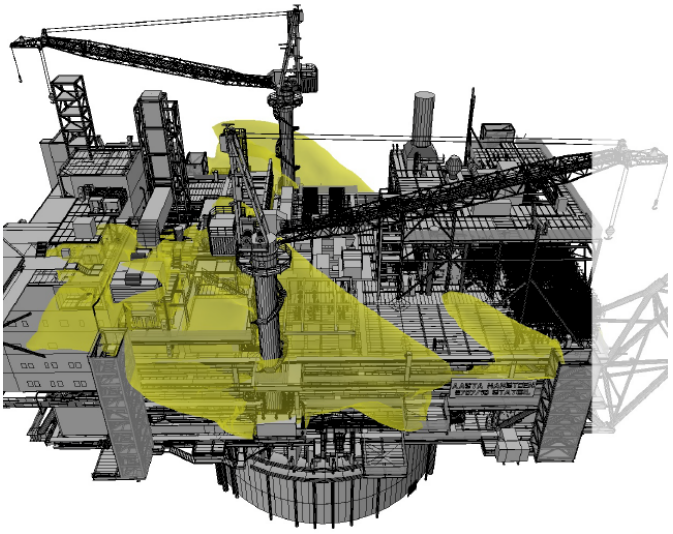

FIGURE 2.2: An example of a leak in main process area. [16]

2.2.4 Ignition modelling

When the hydrocarbon is released, there is a probability for the released gas to ignite causing an explosion and/or fire. The probability of this ignition is time dependent and is, in addition to the type and density of ignition sources in the area, determined by the size of the flammable cloud as a function of time. The sources of ignition can be divided into four different classes:

- **Event ignition** is when the source itself causes both leak and ignition and it is assumed to occur within a few seconds before any significant gas cloud is developed. This leads to fire, but does not contribute to the explosion frequency.
- **Continuous ignition sources** are continuous by having constant or decreasing strength. In this case the ignition occurs immediately after exposure of the ignition source. Therefore, the ignition probability in a time step is proportional to the increase of cloud volume in the time step. Longer exposure time for the same cloud size will not lead to a larger ignition probability, since the ignition model assumes immediate ignition.
- **Discrete ignition sources** exert sparks at random points in time. The probability of ignition from a discrete ignition source in a time step is thus proportional

to the total cloud volume. Thus, a longer exposure time for the same cloud size will increase ignition probability.

- **External ignition** is when the gas leak is exposed to an ignition sources in other areas of the platform. In addition to the ignition sources listed above, other equipments such as cranes, non-electrical equipment and turbine air intakes have a much greater probability for ignition given exposure.

The probability of ignition will depend on the number and type of ignition sources in the nearby area, the probability that combustible gas is exposed to the ignition source and the probability that the exposed combustible gas is ignited.

2.2.5 Explosion analysis

When the right conditions are met and the flammable gas cloud ignites, pressure and drag loads are exerted on the structures in the surrounding area. The results from the gas dispersion analysis and the ignition model are used to obtain dimensional loads, also called the pressure-frequency curves.

Load definition

The loading scenario on an object exposed to an explosion can be divided into two:

- Net reaction force. This is the total load on the object resulting in a net force trying to move/overturn the object. The net reaction force consist of the following components: (a) Form drag $\frac{1}{2}C_d\rho v^2$, (b) inertia drag due to acceleration, (c) combustion effects due to transient changes in density, (d) differential pressure due to static pressure variations and (e) hydro-elastic effect when vortex shedding movement causes increase of drag coefficient when the vortex shedding effect is close to the natural period of vibration.
- Surface load. The force acting on each surface of the object resulting in deformation of that surface.

The total pressure can be split in components of static pressure and dynamic pressure. Static pressure is e.g. the pressure in a volume where there are no pressure waves, so where it is associated with its state and not the motion. Dynamic pressure is the pressure due to the kinetic energy flow.

Explosion simulations

Explosion simulations are in general performed to estimate the pressure and drag loads caused by an ignited gas cloud. The previous analysis of gas dispersion and ignition models are used to obtain pressure-frequency curves. The dimensioning explosion pressure are found by applying the risk acceptance criteria for explosions to these curves. CFD modelling is used to establish the probability distribution of an explosion pressure for a given volume at given target locations, see figure 2.3. A number of scenarios needs to be simulated with various cloud sizes, cloud shapes, cloud locations and ignition locations to get satisfying statistical input.

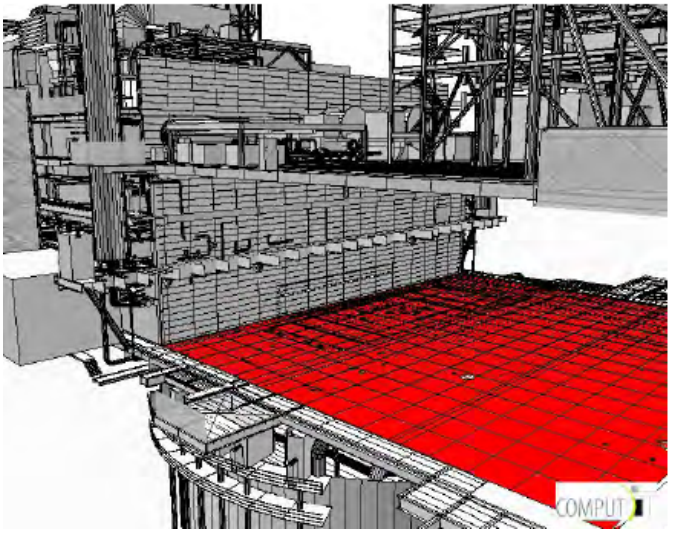

FIGURE 2.3: Cellardeck (equipment removed). [4]

Explosion pressure probability

Different percentiles are established for pressure dependent on the relation between cloud size, pressure and the distribution of deviations. The obtained correlation is used for calculating the pressure frequency curves from the frequency distribution for ignited clouds. Figure 2.4 shows an example of a probabilistic representation of pressure on target areas (located at e.g. main process area), volume of the ignited distributed gas clouds and the corresponding probability for the given cloud sizes. Different pressures for the same volume are found due to the uncertainties that represent the deviations from CFD-simulations and experiments, uncertainty in the transition between inhomogeneous to stoichiometric cloud an uncertainties in the geometry model. The plot illustrates the results of how the 3D surface is represented in 2D (with k-lines) for the main process area. The dots in the pressure-volume plane represent the raw data from CFD simulations.

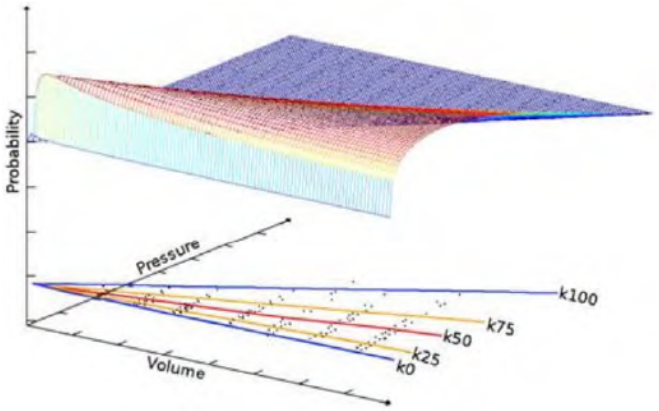

FIGURE 2.4: Example of a probabilistic representation of pressure, volume and probability. [4]

The percentiles $k0$, $k25$, $k50$, $k75$ and $k100$ represents the probability in percentage for the load to be smaller than the actual percentile for a given cloud size.

Duration of load

The full effect of an explosion on a given target location is known by analysing the maximum load and duration of the load over time. The maximum force and the force as a function of time acting on the same target might have different consequences. The duration can be calculated with the following equation:

$$I = \int_{t0}^{t1} p(t)dt \tag{2.2}$$

where I is the impulse, t the time and $p(t)$ the pressure as a function of time. The explanation of the shape of the pressure as function over time will be described later on. Figure 2.5 illustrates the shape of the pressure as a function of time for a panel based on the simulations. This shape is close to a triangle and therefore can be simplified and be approximated by the following equation:

$$\Delta t = \frac{2I}{p_m} \tag{2.3}$$

where p_m is the maximum/minimum pressure. The duration will then be calculated for all simulated scenarios according to this equation and plotted in a pressure duration plot to come up with a relation between pressure and duration.

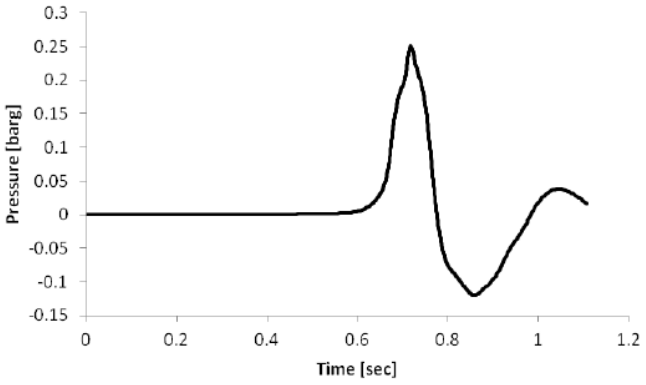

FIGURE 2.5: Example of a pressure as a function of time for one panel for one of the explosion simulations of the main process area. [4]

2.2.6 Pressure-frequency distribution

The pressure-frequency distribution is used to eventually establish the response of the structure. The main results from probabilistic explosion analysis are based on pressure-frequency curves for different targets. In order to produce the pressure-frequency curves information about the leak picture and gas dispersion needs to be combined. The main steps for computing this are:

- Distributing the leak frequencies to different leak categories.
- Associate relative leak probabilities with the different areas which the gas dispersion scenarios represent.
- Associate relative probabilities to the segments.
- Use these results along with the results from the explosion simulations as input to the ignition model.

Based on these frequencies, different pressures are calculated for a target and this is represented in a cumulative pressure-frequency plot. From this Dimensioning Accidental Load (DAL) are obtained. DAL refers to the loads with an annual frequency less than 10^{-4} that the structure must withstand as a minimum in order to meet the risk acceptance criteria. In addition, a Design Accidental Load is chosen as the basis for design to minimal be capable of resisting the DAL.

2.3 Pressure-time profile

The theoretical and computational models are often started with idealising the explosion. For a detonation this means an instantaneous release of energy from a point source in a free field. An analytical solution is provided in the form of the Friedlander curve, figure 2.6. Realistic impulses are in practice different than the Friedlander profile, because the effect of reflecting surfaces as ground, walls and objects are not accounted, which produces complex wave patterns.

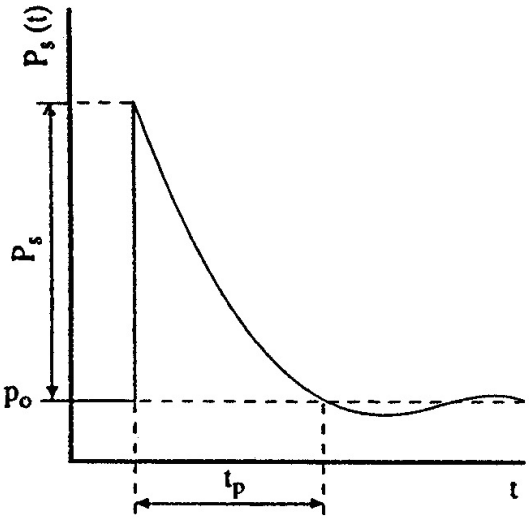

FIGURE 2.6: Shock wave pressure profile, where p_o = initial pressure, P_s = peak side-on overpressure and t_p = duration of positive phase. [6]

Friedlander [7] suggested that this shape could be described by an equation in the form of:

$$P(t) = P_s e^{-\frac{t}{t^+}} \left(1 - \frac{t}{t^+}\right) \tag{2.4}$$

where P is the overpressure at a fixed location, P_s is the peak overpressure, t is the time after the arrival of the primary shock at that location and t^+ is the positive duration. This simple two-coefficient relationship has long been known to be an excellent descriptor of overpressure time-histories produced by a variety of explosives over a wide range of peak over-pressures. However at peak over-pressures above 1 atmosphere $\approx 100\ kPa$ the Friedlander equation is no longer accurate enough to describe the pressure–time history, so another coefficient α is introduced. This is shown in figure 2.7 by Dewey McMillin & Associates [5]. The modified Friedlander equation becomes:

$$P(t) = P_s e^{-\alpha t} \left(1 - \frac{t}{t^+}\right) \tag{2.5}$$

Where α is the shape factor, between 0.1 and 10.

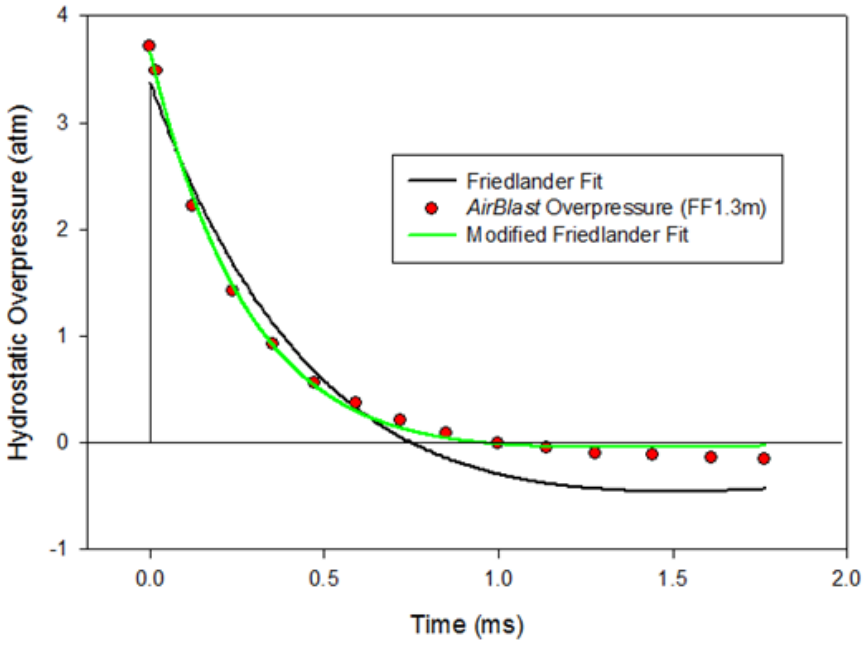

FIGURE 2.7: AirBlast is an interactive data base of blast wave properties provided by Dewey McMillin & Associates [5].

The above is valid for a detonation, but in case of a deflagration explosion the shape of an idealized pressure-time profile is as shown in figure 2.8. The build-up time of the pressure is longer and the peak pressure is lower. This type of profile is common in a hydrocarbon explosion.

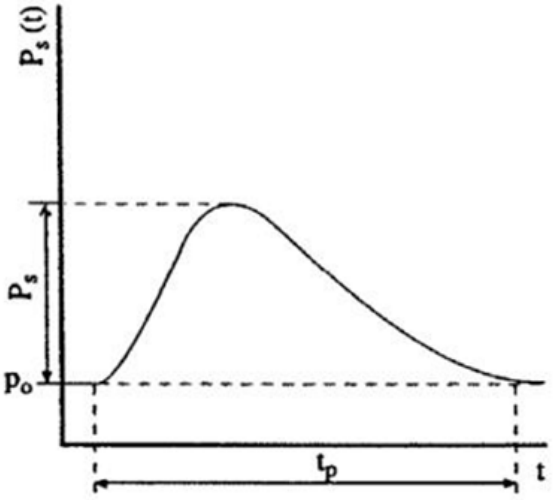

FIGURE 2.8: Idealized pressure-time profile of a deflagration. [6]

Bakri and Watson [3] cited in Fung and Chow [8] showed that further simplification can be made. They made a comparative study on the response of a slab subject to four different type of blast loading shown in figure 2.9. The actual pressure-time profile that was obtain in an experiment is tried to be approximated with each loading type. The lines I, II and III assume linear decay of the loading and ignore the negative phase. Line I uses the same peak overpressure and positive time duration as the actual loading. Line II uses the same peak overpressure, but adjusts the positive phase duration in order to preserve the same impulse as the actual loading. Line III considers only the actual positive phase of the loading and line IV uses the full blast load in both the positive and negative phases. The results showed that line I over predicted the slab response while lines II and III, both having the same impulse, gave similar responses lower than that of Line I. Line IV gave the best prediction for the deflection-time history. These observations suggest that in order to accurately predict the responses of blast loading on structures the negative phase of blast pressure is essential. An overestimation can be considered in a preliminary study by neglecting the negative phase. This will be a safer approach since the blast loading is an uncertainty.

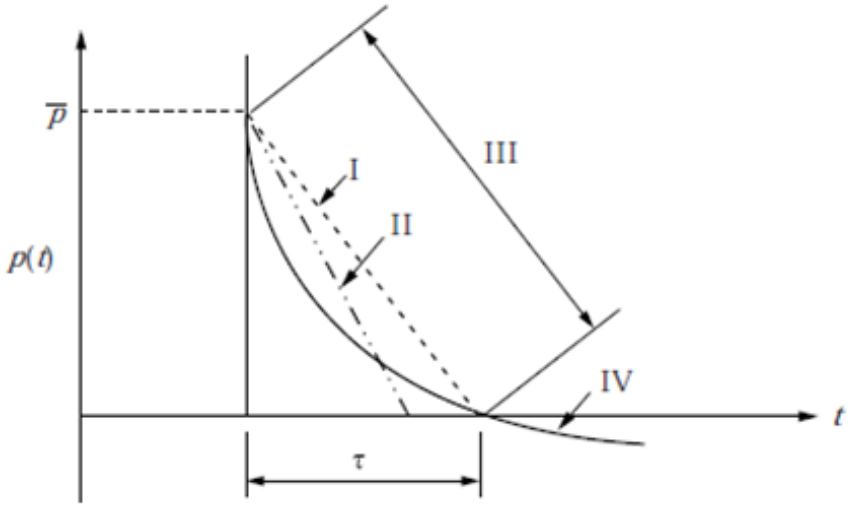

FIGURE 2.9: Different type of blast simplifications. [8]

2.4 Conclusion and discussion

A deflagration is, due to the relative slow energy release of oil/gas, the most likely type of explosion type for the topside structure. However the transition to detonation, which leads to higher pressures should not be neglected.

Furthermore, it was shown that the procedures to determine the blast loads for engineering purposes are based on probabilistic explosion analysis. The analysis consist of establishing the geometry of the structure, the leakage scenarios, cloud size distribution and ignition.

Also, based on probabilistic explosion analysis and studies from Friedlander, Bakri and Watson the blast loading can be simplified. In engineering application the blast loading can be modelled by assuming linear lines. The studies showed that it is acceptable to define the loading as linear triangular lines. Based on this simplifications, duration for the blast loading can be found and used for further analysis. In addition, these observations from Bakri and Watson suggest that the negative phase of blast pressure is important in order to predict accurately the responses of blast loading on structures. This is also done in the Aasta Hansteen project, see figure 2.10 for an example of a blast load.

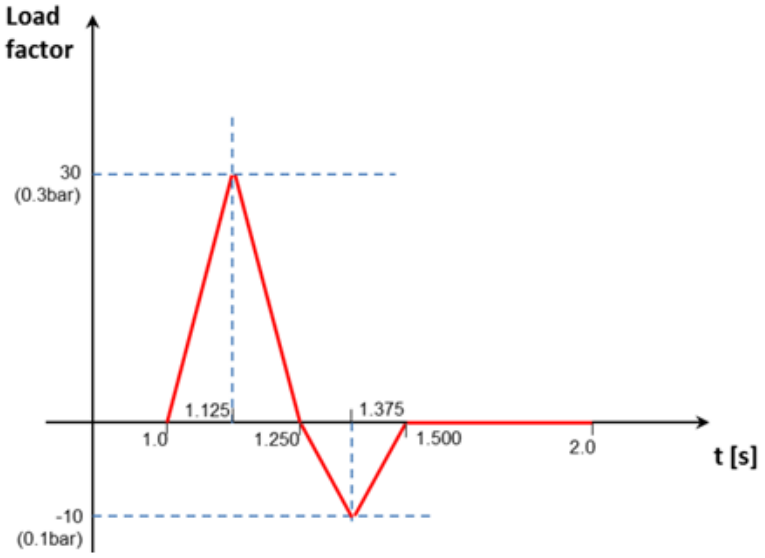

FIGURE 2.10: Example of a blast pulse load profile for 250 ms duration used for Aasta Hansteen. [10]

For the next chapter the shape of the blast loading will be the same as shown above. The values of the positive and negative peak will only change.

Chapter 3

Plastic Analysis

The first part of this chapter consist of modelling the material behaviour. This is done for analytic calculations and for calculations in SACS (Structural Analysis Computer Software), which is used by CB&I. SACS is a widely used software in the offshore industry to model and analyse offshore structures. SACS provides the user the ability to dynamically iterate designs to perform advanced analysis, comply with offshore design criteria, and visualize results. More information about SACS and the analysis method can be found in Appendix A. The material modelling in SACS is made the same when a comparison is made between the results of SACS and the results of the analytic analysis. Furthermore, an example of a comparison between a static elastic and static plastic behaviour of a frame structure is performed. This is to show the influence of the plastic reserve capacity of the material which is not taken into account in linear calculations. The next part consist of the dynamic behaviour of the same frame structure. The idea here is to compare different plate girder-column stiffness ratios and the impact on the linear and non linear results in order to propose a certain amount of exceedance of the UC.

3.1 Modelling of material behaviour

The relations between stress and strain for a material can be determined with an uniaxial tensile experiment. For steel, the idealised shape of this relation would be like illustrated in figure 3.1a. However this relation is often further simplified for analytic calculations and even for FEM software with limited options to model the material behaviour. The diagram is further idealised to elasticity with ideal plasticity for analytic calculation, see figure 3.1b. Furthermore, in the last diagram the elasto-plastic material with strain hardening is shown. This material behaviour is used in SACS for non linear calculations.

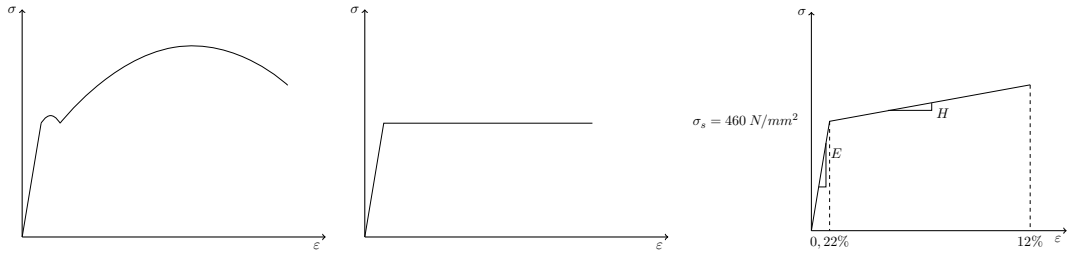

(A) Idealised stess strain relation for steel (B) Elasticity with perfectly plasticity (C) Elasticity with strain hardening

FIGURE 3.1: Idealised stress strain relations

3.2 Static plastic behaviour of beams

For simple hand calculations the material model is considered to be elastic with perfect plasticity, figure 3.1b. The distribution of stresses for a plate girder is drawn below:

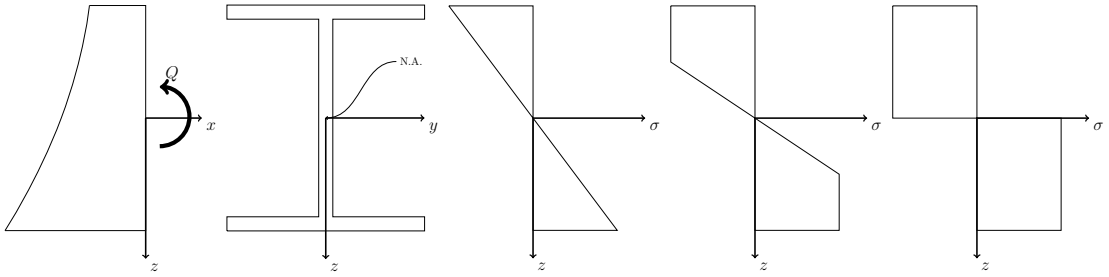

(A) (B) (C) (D) (E)

FIGURE 3.2: Plastic zone development subjected to a pure bending moment. (a) Side view of girder ; (b) symmetric cross section; (c) elastic stress distribution; (d) elastic perfectly plastic stress distribution; (e) fully plastic stress distribution.

The relation between moment and curvature is valid until yield stress reached σ_p. For elastic perfect plastic relation seen in 3.1b the yield stress σ_y is equal to the plastic stress σ_p. The strain distribution remains the same when the moment is further increased. The equilibrium is also satisfied during plastic stage, but what changes is the relation between stress and strain. The relation between stress and strain for elasticity with perfectly plasticity can be calculated by the following equations:

$$\sigma = E\,\varepsilon \quad for \quad |\varepsilon| < \varepsilon_p \tag{3.1}$$

$$\sigma = \pm\sigma_p \quad for \quad |\varepsilon| \geq \varepsilon_p \tag{3.2}$$

The elastic and plastic moment in the cross section are given by:

$$M_e = \sigma_y W_e \tag{3.3}$$

$$M_p = \sigma_p W_p \tag{3.4}$$

The elastic section modulus is described as $W_e = \frac{I}{c}$ where I is the second moment of area and c is the distance from neutral axis to outer fibre of the cross section. The second moment of area for a plate girder as seen in figure 3.3 is described as:

$$\begin{aligned} I_{zz} &= I^{web}_{zz(center)} + 2 \times \left(I^{flange}_{zz(center)} + I^{flange}_{zz(Steiner)}\right) \\ I_{zz} &= \frac{t_w\,(d - 2\,t_f)^3}{12} + 2 \times \left(\frac{w\,t_f^3}{12} + \frac{w\,t_f\,(d - t_f)^2}{4}\right) \end{aligned} \tag{3.5}$$

The plastic section modulus for the symmetric plate girder is given by:

$$W_p = w\,t_f(d - t_f) + \frac{t_w(d - 2\,t_f)^2}{4} \tag{3.6}$$

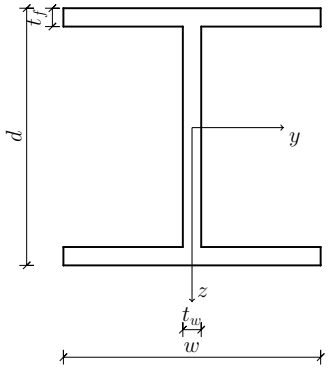

FIGURE 3.3: Symmetric plate girder

When the stress is homogeneously spread across a cross section (e.g. tension) then the plastic capacity is equal to the elastic capacity. This means there is no reserve capacity left. In case of non-homogeneously distributed stress (e.g. bending) the ratio of plastic to elastic capacity is equal or bigger than the shape factor, k depending whether the structure is statically determined or undetermined. An undetermined structure has a higher ratio of plastic to elastic capacity. The shape factor is for the perfectly plastic material model defined as [15]:

$$k = \frac{W_p}{W_e} = \frac{M_p}{M_e} \tag{3.7}$$

The structure in figure 3.5a is second order statically indeterminate structure due to the absence of a horizontal load. If now the comparison is made for static analysis with and without plastic capacity, then the gain of incorporating plasticity will be evident. It is assumed that the moment-curvature characteristics is bilinear as shown in figure 3.4.

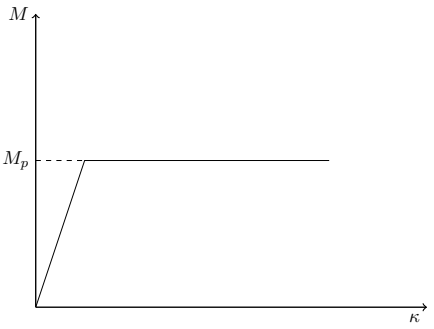

FIGURE 3.4: Moment and curvature relation

The frame structure in figure 3.5a loaded by the uniform surface load q_d responds linear elastic until in the middle of the plate girder the bending moment becomes equal to the plastic moment M_p. When this occurs a plastic hinge will developed on that spot and further load increment will lead to an increase of the moments somewhere else, in this case at the left and right side of the beam. Thereafter, plastic hinge at that location will also be developed. This process continues until a mechanism is formed, which means that the deformation of the structure is unlimited without any load increase. A mechanism for this structure will be developed after three plastic hinges.

For the structure in 3.5a the bending moment diagram is given in figure 3.5b. When the EI of the beam and columns are considered equal and h and l have the same size then the moments can be described as (see Appendix D):

$$M_B = M_D = \frac{ql^2}{18} \tag{3.8}$$

$$M_B = M_D = \frac{ql^2}{18} \tag{3.9}$$

where the maximum bending moment located in the middle of the beam described as:

$$M_C = \frac{5\,ql^2}{72} \tag{3.10}$$

After the formation of plastic hinges seen in figure 3.5c the moments can be described as $M_B = M_C = M_D = M_p$ and $M_A = M_E = \frac{M_p}{2}$. The resulting collapse load is found by use of the virtual work principle.

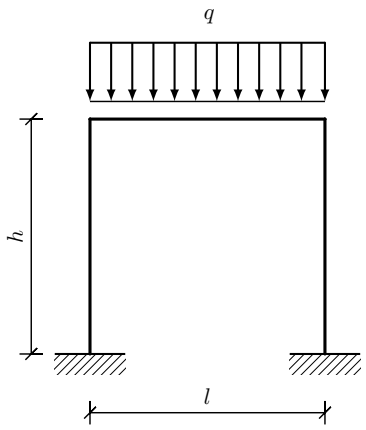

(A) Frame structure with a distributed load

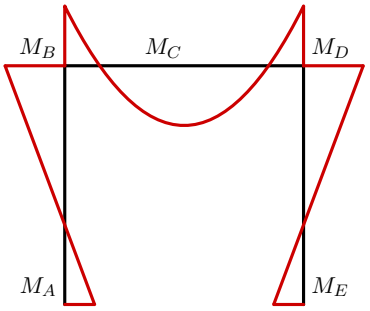

(B) Elastic bending moment diagram

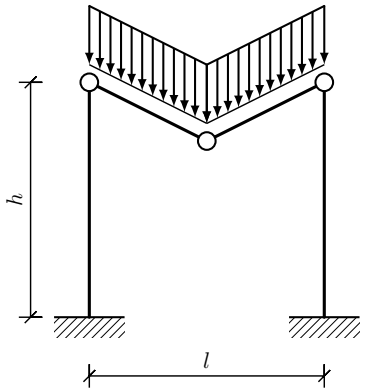

(C) The mechanism of the structure

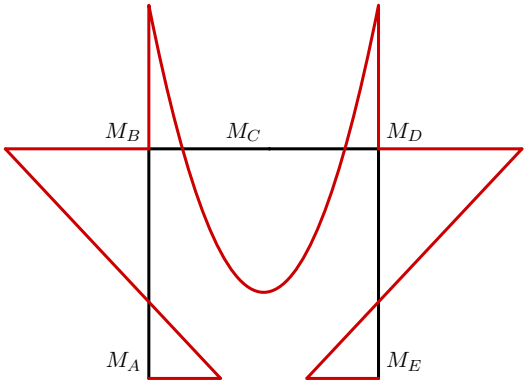

(D) Bending moment diagram for collapse

FIGURE 3.5: Elastic and elastic-plastic analysis of a frame structure loaded by a uniform distributed load.

$$4M_p\theta = \frac{ql^2}{4}\theta \tag{3.11}$$

Eliminating θ and rewriting the equations becomes:

$$q = \frac{16M_p}{l^2} \tag{3.12}$$

In equation 3.10 is shown that corresponding load for the maximum elastic bending moment is given as

$$q = \frac{72M_p}{5l^2} = \frac{14,4M_p}{l^2} \tag{3.13}$$

So, the ultimate load bearing capacity obtained by allowing plasticity is $\frac{16}{14,4} = 1,11$ times higher than the value according to the elasticity theory. Furthermore since M_p is related to the cross section of the beam the increase of load bearing capacity is even more. For this structure it is $1,11k$ where k is in this case based on the cross section of the plate girder. For example $k = 1,15$ gives an increase of $1,11 \times 1,15 \approx 1,28$, thus an increase of about 28%.

Note that buckling does not occur, because the loads in these examples are small compared to the required buckling force. Furthermore, the effect of axial load on plastic moment is neglected. In practice this axial load would only cause small area of section to yield and the effect on W_p is minor.

The result of these calculations are compared with SACS to find the right input parameters in the software for later dynamic analysis. First the calculation method for the structure in 3.5a written previously will be specified with numbers. The dimensioning values, like the diameter and thickness of the tubular column are chosen in such a fashion to be able to obtain equal bending stiffness for beam and column. The values are for comparison purposes and are not used afterwards.

TABLE 3.1: Values for comparison calculation

length $l\,(m)$	height $h\,(m)$	diam. col. $D\,(cm)$	col. thickn. $t_c\,(cm)$	width fl. $w\,(cm)$	fl. thickn. $t_f\,(cm)$	height fl. $d\,(cm)$	web thickn. $t_w\,(cm)$	yield stress $\sigma_y\,(N/mm^2)$	Young's mod. $E\,(N/mm^2)$	Poisson's ratio
9	9	100,9	5,968	48	2	155	3,1	460	210.000	0,3

The resulting moment of area for the column and beam are equal to 2013124 cm^4 and since the length and height of the structure is equals, therefore the use of equation 3.13 is allowed. The maximum bending moment described using equations 3.6

$$M_p = \sigma_p W_p = 460 \cdot 10^3 \times 32358,8 \cdot 100^{-3} = 14885,0\,kNm \tag{3.14}$$

This gives according to equation 3.13 a distributed collapse load of

$$q = \frac{16 M_p}{l^2} = \frac{16 \cdot 14885}{9^2} = 2940\,kN/m \tag{3.15}$$

A comparison of nominal stress at one location on the structure is made to verify the accuracy of the software at given options and settings for the collapse module. First a static elastic calculation is performed to determine a sufficient mesh size and other settings. The self-weight, which is automatically taken into account is eliminated by multiplying the self-weight by a very small number. The length of the members are set to 1 meter, the fixity of the supports to 111110 (see Appendix A) and the beam and columns to 212000. The applied distributed load is set to 4000 kN/m, this value is chosen big enough for later use on collapse analysis. The results for linear analysis will not be influenced by this load. The analytical calculated stress is compared to the stress found in SACS to determine whether the solutions are the same. The maximum nominal stress for this structure is given by the following equation:

$$\sigma_x = \left|\frac{M_y}{W}\right| + \left|\frac{F}{A}\right| \tag{3.16}$$

The moment in the middle of the beam is given by equation 3.10 in:

$$M = \frac{5 \cdot 4000 \cdot 9^2}{72} = 22500\,kNm \tag{3.17}$$

and the horizontal force for this structure is equal to:

$$F = \frac{ql}{12} = \frac{4000 \cdot 9}{12} = 3000\,kN \tag{3.18}$$

The area for the plate girder described before results in $A = 660,1\,cm^2$ and $W_y = 25975,8\,cm^3$. Filling these values in equation 3.16 gives:

$$\sigma_x = \frac{22500 \cdot 10^6}{25975,8 \cdot 10^3} + \frac{3000 \cdot 10^3}{660,1 \cdot 10^2} = 911,6\,N/mm^2 \tag{3.19}$$

The stresses found in SACS report are equal to:

$$\sigma_x = flexural\ stress + axial\ stress = 850,82 + 44,94 = 895,8\,N/mm^2 \tag{3.20}$$

This stress is the actual stress and not the allowable stress which would be obviously lower than the yield stress. The difference between the analytical calculation and SACS is due to the fact that SACS take the stresses at the end of the middle member. Since the middle member takes the stress half meter next of the centre, the moment there is lower causing a lower bending stress. After adding extra mesh in the middle of the beam the nominal stress becomes practically the same.

Now, the same calculation has been done in SACS to find out for which settings e.g. the number of member segments is sufficient to find the collapse load matching the analytical collapse load. The definition of collapse in SACS is described in Appendix A, but a summary of it is as follows. The structure is considered to be collapsed when a mechanism is formed, which is signified by a non-positive definite stiffness matrix. A mechanism takes place due to plastic hinges formation in the structure in combination with a disconnected member or by a disconnected member by itself. A member disconnects (ruptures) when the maximum allowed strain is exceeded. The structure is also considered to be collapsed when a very large displacement, defined by the user, occurs for a small increase in load. This deflection corresponds to the largest joint displacement in the whole model. When one of these occurs the programs stops the analyses and reports collapse.

The applied distributed load is also set to 4000 kN/m, this value is divided in increments of 1000 load steps to find out the collapse load in the results. The static full plastic collapse/pushover analysis is performed with an additional collapse input file in the static analysis. The most settings are leaved as default. The maximum allowed ductility

is set to the proportional limit strain of 0,22% to come as close to the analytic calculation. However it should not make too much of a difference since there is no strain hardening. Some of the values in the collapse input file are as follows:

TABLE 3.2: Values Collapse input file

Max. iterations per load increment	50
Number of member segments	1
Max.No. of member iteration	50
Deflection tolerance	0,01 (cm)
Rotation tolerance	0,001 (rad)
Member deflection tolerance	0,01 (cm)
Collapse deflection	1000 (cm)
Strain hardening ratio	0

The number of member segments is an important parameter for the collapse results. The number of member segment is 8 by default. This means each member is discretized by using sub-segments along the member length. The segmented elements is then dived into sub-elements based on the cross section. The number of sub-elements for a plate girder is seven. For any stiffness iteration, each sub-element is checked for plasticity using von Mises stress surfaces. When the material elastic limited defined in the input file is exceeded, due to high stress in the cross section, the sub-element is then considered to be plastic, thus allowing for gradual plastification of the beam cross section. Table 3.3 shows different number of member segments to see what kind of influence it has on the corresponding collapse load.

TABLE 3.3: Number of member segments

Number of member segments	Resulting collapse load (kN/m)
1	2740
2	2656
4	3112
6	3240
8	3296
10	3280
12	3284
24	3312

It can be seen that the number of member segments of 1 and 2 results in a collapse load lower than the analytical collapse load of $q = 2940\,kN/m$. This is a bit odd, because SACS takes also the axial forces into account which contributes to the deformation. The expectation would be that the collapse load in SACS should be slightly higher for this scenario. Therefore using lower number of member segments for analysis leads to less

accurate results. Also the prediction of a plastic hinge along each element would be less accurate as no (sufficient) checks are conducted along the element length (Appendix A). Knowing this and the results shown in table 3.3, means that the number of segments should be 4 or above. However, when these results are compared with hand calculations one sees approximately 10% difference between the analytical and SACS collapse load.

The first order calculation does not take the influence of the deformed shape into account. The deformation due to the shear force are thus not taken into account, which is justified for slender beams. On the other hand when the elastic deflection of the middle of the beam in SACS (at lower loads when it is still elastic) is compared to the hand calculation there is no significant difference, but there is a tensile force that is caused by the columns that are bent in-worth. This reaction force will cause an opposite bending moment which will lead to higher collapse load capacity. However, like mention before the displacement that determined the arm of the force is not big enough to significantly increase the collapse load. Furthermore, local buckling effect are disabled, which has also not been taken into account for the analytic calculation. Also strain hardening is not the explanation, since that is also been disabled. All in all the reason why the collapse load in SACS is higher has not been fully understood, but since the number of member segments 1 and 2 does not predict a hinge accurately the number of segment for further analysis seen in the next paragraph will be set to 4, which seems a good trade-off between accuracy and computation time.

Furthermore, the tolerances in the input files needs attention. In the static plastic analysis the software uses iteration in each load step. In these iterations the node displacement and node rotations are improved until al equations are fulfilled to sufficient degree of accuracy. The required accuracy or tolerance is input as a node displacement difference between two subsequent iteration or a node rotation difference between two subsequent iterations. In the previous model the values for these parameters are given in table 3.2. It is important to set these values properly. For example, very large tolerances leads to just one iteration per load step and inaccurate results. In one case the result was about 50% off the correct value.

3.3 Dynamic plastic behaviour of beams

For a dynamic plastic analysis the inertia force has to be taken into account. This can be done analytically, but SACS is used for the dynamic analysis. Again, blast load is assumed to be equally distributed along the length of the beam. In this paragraph the dynamic plastic relation between the column and beam will be treated. The stiffness ratio between the column and beam is changed to analyse the difference between the elastic dynamic and plastic dynamic calculations, in terms of stresses and unity checks corresponding to collapse. The analysis is therefore divided into two parts. The first part consist of an elastic analysis and the second part a plastic analysis. The material model used for the plastic analysis in SACS is illustrated in figure 3.1c. This material model is a more accurate representation of the real behaviour of steel. This material model is also used in the EPC phase of projects. SACS does not need additional input for the material model for the elastic analysis, since the calculations are linear.

Figure 3.6 shows a schematic view of the model used in SACS. The length and height of the structure is kept constant for each cases, which is 18 m for the length and 9 m for the height. To begin the modelling in SACS, a couple of cases which represent different stiffness ratios between the column and beam has to be set up. Afterwards the results of this analysis will be shown. This time the self-weight of the structure is taken into account and the dynamic load is the same for all the cases. The peak positive loading is 270 kN/m and the negative peak loading is 90 kN/m of the blast loading. Since, the modelling is done in 2D the blast pressure of 0,3 bar (30 kN/m^2) is multiplied by 9 m to represent the depth of the structure. The total duration of the load inclusive negative phase is 500 ms. Also a static distributed load is applied to represent the equipment weight and to simulate a more realistic scenario. The static load of 110 kN/m is applied exclusive the self-weight, which changes for each case. The difference of self-weight between the cases are too small compared to the static and dynamic loads to have a significant change on the results. Again all elements have a length of 1 meter. Table 3.4 shows the properties for the different cases.

FIGURE 3.6: Model for dynamic analysis

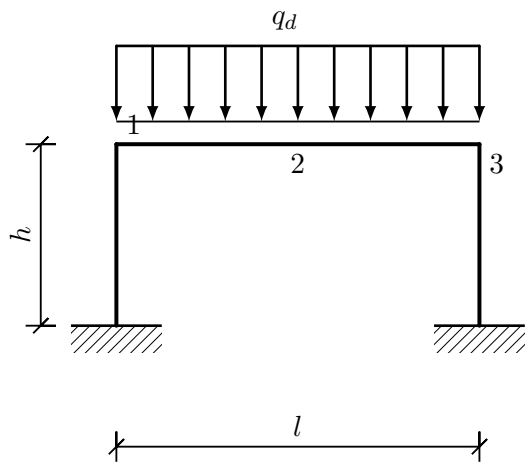

Table 3.4 shows the dimensions and corresponding bending stiffness for each case. For the first five cases the beam size is kept the same, but the column size is decreased. For the last three cases the beam size is changed and the column size is kept the same. The change of the column and beam sizes was stopped until collapse occurred.

TABLE 3.4: Stiffness ratios between column and beams

	Plate girder						Column			
Case	Width (cm)	Flange thickn. (cm)	Height (cm)	Web thickn. (cm)	Cross section area (cm^2)	Inertia (cm^4)	Diameter (cm)	Tickn. (cm)	Cross section area (cm^2)	Inertia (cm^4)
1	60	4	120	2	704	1849514,7	160	6	2902,8	8618507,1
2	60	4	120	2	704	1849514,7	140	5,5	2324,0	5263989,8
3	60	4	120	2	704	1849514,7	120	4,8	1737,2	2886768,1
4	60	4	120	2	704	1849514,7	100	4	1206,4	1392152,8
5	60	4	120	2	704	1849514,7	80	3,2	772,1	570225,8
6	60	4	100	2	664	1236341,3	100	4	1206,4	1392152,8
7	60	4	110	2	684	1525828,0	100	4	1206,4	1392152,8
8	60	4	130	2	724	2208401,3	100	4	1206,4	1392152,8

For a dynamic analysis requires SACS several other input files such as Dynpac to generate the dynamic characteristics including the mode shapes, natural periods and internal load and stress vectors for the structure. This is for the elastic and plastic analysis the same, see Appendix A for the required modules for each type of analysis. The important input parameter for Dynpac is the number of modes. For these structures it is chosen for 32 modes, because then the results shows that at least 98% cumulative mass is participating. In general the more is better, however it takes more time to calculate. The applied static load is also converted to mass at each node. Afterwards the Dynamic Response module is used to compute the dynamic response of the structure subjected to excitation exerted by the blast load. A structural damping of 2% was applied for the elastic and plastic analysis. For the plastic calculation this analysis is the last step

and it requires a collapse input file to conduct a non-linear analysis. In case of elastic analysis the Dynamic Response module performs only linear analysis. Thereafter the Combine module is used to combine the static results and the (linear) dynamic results of the same model into one solution file. Following the Postvue module to review the analysis.

The input for the collapse file is almost the same as before. However the strain hardening ratio, H is set to 0,0034. This ratio in combination with the plastic strain determines the fracture stress. The number of member segments is still 4 and the maximum ductility allowed is 12%. Also, buckling effect are taken into account in this analysis.

TABLE 3.5: Collapse input file for dynamic plastic analysis (short)

Max. iterations per load increment	50
Number of member segments	4
Max.No. of member iteration	50
Include local buckling effects	Yes
Local buckling method	ISO 19902 section 13.2.3.3
Deflection tolerance	0,01 (cm)
Rotation tolerance	0,001 (rad)
Member deflection tolerance	0,01 (cm)
Collapse deflection	1000 (cm)
Strain hardening ratio	0,0034

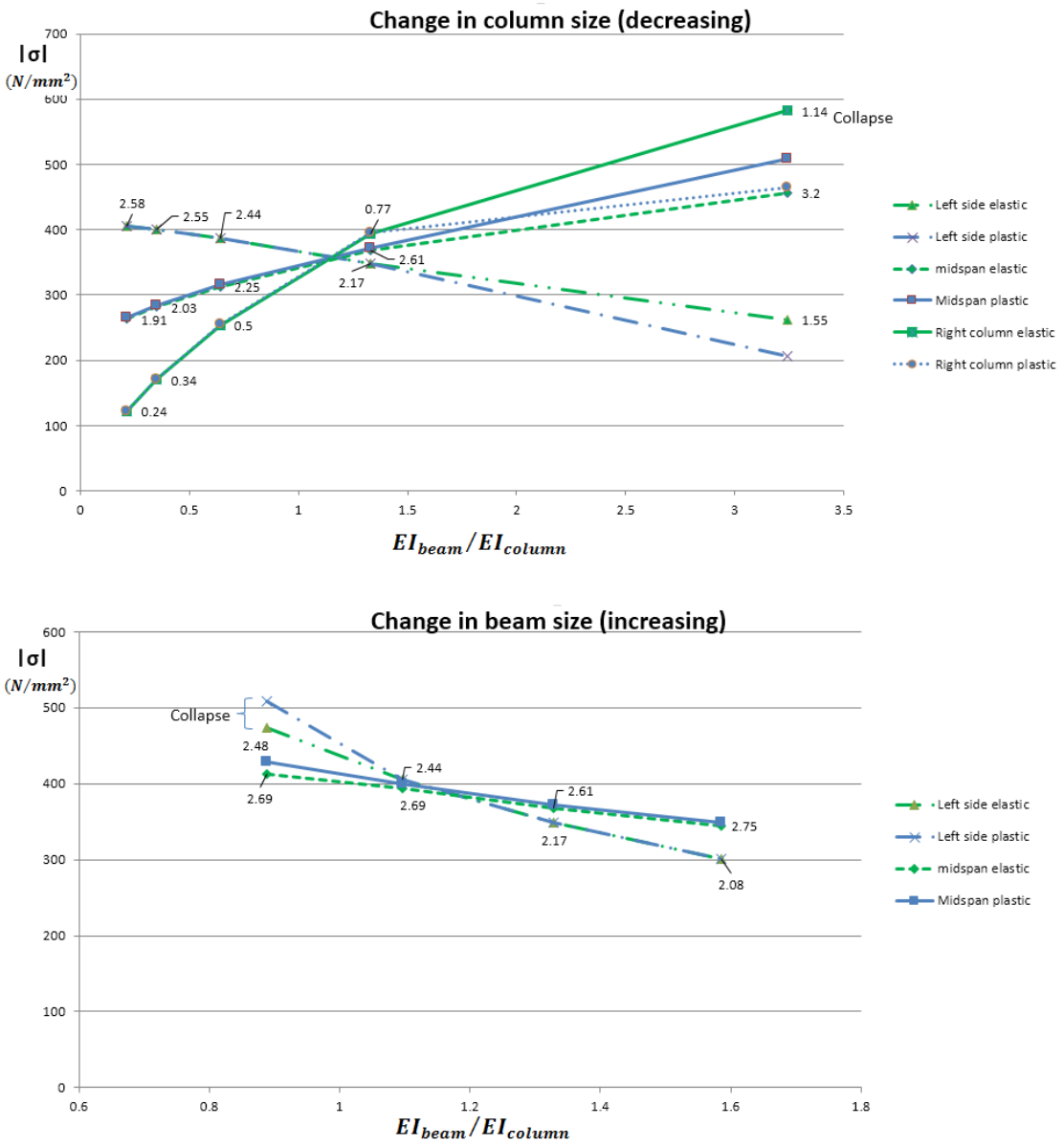

FIGURE 3.7: Results of the stiffness ratios in relation to the elastic and plastic stresses

After obtaining the elastic and plastic results of the different cases, the axial and flexural stress are extracted from SACS for the left side of the beam member (number 1 in figure 3.6), the midspan member (number 2 in figure 3.6) and upper right column member (number 3 in figure 3.6) and plotted against the bending stiffness ratio between the beam and column. The mentioned locations were chosen based on the occurring highest stresses. The results are illustrated in the figure 3.7. The top figure corresponds to the first five cases where the columns size was changed and the bottom figure corresponds to the cases 4, 6, 7, and 8 where the beam size was changed. The reason why the results of location 3 is not taken for the second graph is because the columns size does not play a important role on the cause of collapse, since it was kept the same. The vertical axis is the sum of the axial and flexural stress and the absolute values are plotted. The absolute

values are plotted because of the sign difference between the flexural stress on location 1 and 2. The green lines represents the elastic analysis and the blue lines the plastic analysis. The numbers at the elastic lines shows the corresponding UC value. The UC is the ratio between the (sum of the) relevant actual stress(es), such as axial stress due to compression and flexural stress due to bending and the (sum of the) allowable stress(es).

Most of the stresses shown in the graph are lower than the yield stress yet still have high UC. The reason for this is that the allowable stresses is not equal to the yield stress, but much lower for these cases, which are reduced by safety factors in the code checks and also reduced to prevent buckling by limiting the maximum allowable stress to the appropriate buckling stress. Also there is a reduction due to the complex loading condition (normal and shear stresses) where this mix of stresses leads to yielding before the yield stress is reached. As seen at the previous paragraph it is normal for the elastic calculations to have higher stresses than the yield stress, because the software calculates the acting stresses separate with the allowable stress. The stresses for the plastic analysis does exceed the yield stress. This is because of the strain hardening allowing for higher stresses.

Collapse occurs for case 5 and 6. The structure in case 5 collapses due to local buckling (see figure C.5 in Appendix C) of the right upper column in combination with plastic hinge formation in the midspan of the beam. The structure in case 6 (see figure C.6) collapse due to the high stresses at the left and right side of the beam.

The results shows that when the column is stiff compared to the beam ($\frac{EI_b}{EI_c} < 1$) the stresses are more concentrated at the side of the beam and when the beam is more stiff compared to the column ($\frac{EI_b}{EI_c} > 1$) the difference between the stress at the side of the beam and midspan becomes smaller. And regarding case 5, where the structures collapses, the right column and midspan have a higher stress compared to the left side. This can also be seen for the lower graph where the size of the beam is changing, except the stress for ($\frac{EI_b}{EI_c} < 1$) is too high and the structure collapses. Nonetheless, the same behaviour is noticed. So, when the bending stiffness of the column is decreasing then this leads to the redistribution of the stresses from the lefts side of the beam to the midspan.

Also, both the graphs shows that the stresses for elastic and plastic analysis are the same for cases where the structure did not collapse (case 1, 2, 3, 4, 7 and 8). For case 5 the left side of beam and the right upper column side shows 20% more stress for elastic analysis compared to plastic analysis and 11% increased stress for the midspan for plastic analysis compared to elastic. This means that when plasticity is allowed, then the stresses are redistributed to the midspan leading to an increase of stress there and decrease of stress at the side of the beam. For case 6 (bottom graph) the plastic analysis shows approximately 7% increase in stress for the left side of the beam compared to elastic analysis. For the midspan there is only 4% difference between plastic and elastic analysis.

In order to tolerate UC exceedance above 1 in a linear blast analysis it is important to look for the highest UC value of the structure, whether it is located on the beam or column and not separately for each member. For example case 5 shows UC of 1,14 for the column, but the UC for the middle of the beam is 3,2 which is one of the cause leading to collapse in the non linear analysis. Also it is important to determine whether the members which exceeds UC of 1 have a slender cross section. When this is the case the allowable stress will be much lower than normal, which causes a high UC in the linear analysis. So, if one observes the graphs it can be seen that despite the high UCs for all the cases, when all the stresses on different locations of the structure in the linear analysis are below the yield stress (460 N/mm^2) the structure will not collapse in a plastic analysis.

The conclusion is that an UC of 1,14 in an elastic dynamic analysis can already lead to collapse in a plastic dynamic analysis. However, once an UC of 2,75 in an elastic dynamic analysis did not lead to collapse in a plastic dynamic analysis. The rule that an UC of 1,30 is acceptable is neither economical nor always safe and therefore a generalisation of 30% increase in UC should not be used, but has to be decided for each situation.

Chapter 4

Sensitivity of strain rate

This chapter consist of the sensitivity of strain rate on structures and how this effect can be implemented in linear calculations.

The yield criteria which govern the plastic flow is assumed by SACS to be independent of the rate of strain, $\dot{\varepsilon}$. However it is known that some materials are sensitive to the rate of strain. When the plastic flow of a material is known to be sensitive to strain rate it is so called a viscoplastic material. Considering the situation where the blast load is causing a sudden increase in load will lead to a change in strain in the material and hence a rate of strain. Marsh and Campell [11] have conducted several experiments to illustrate the effect of the strain rate. The results of such an experiment where the effect of different strain rate for uniaxial compression is shown in figure 4.1.

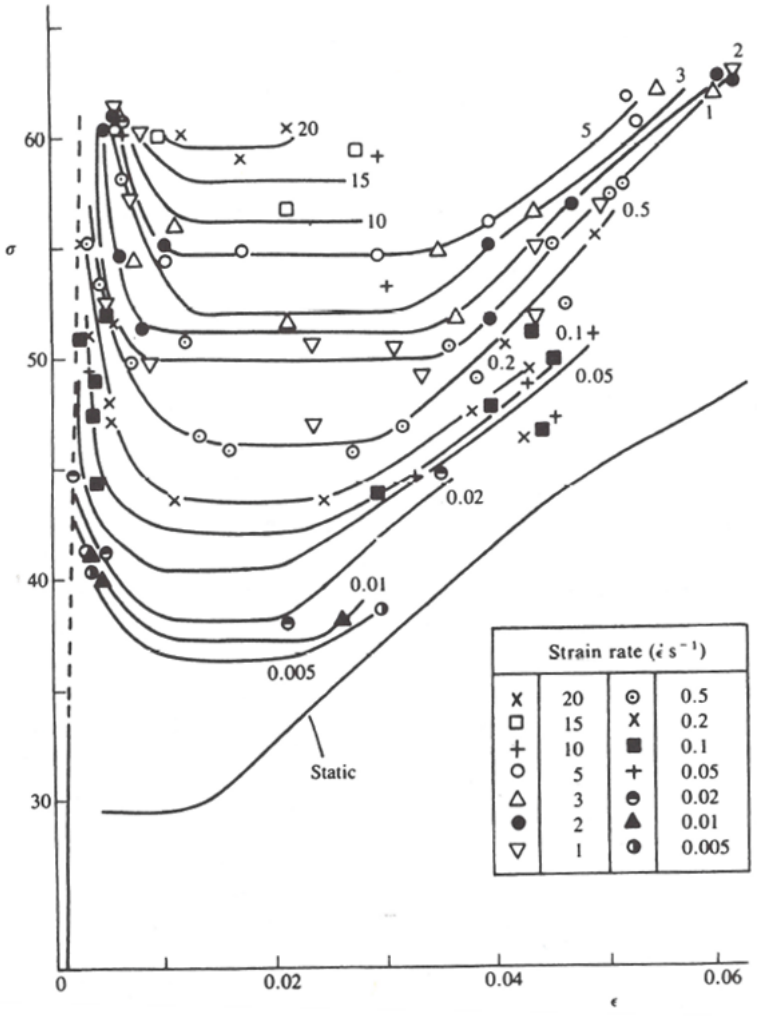

FIGURE 4.1: Stress-strain curves for mild steel at various uniaxial compressive strain rates. 1 unit of ordinate is $10^3 lbf/in^2$ or $6.895 N/mm^2$. [11]

One can see that this material is sensitive to higher strain rates. The dynamic flow stress is much higher than the static flow stress. Hence the importance of this phenomenon for situations such as a blast loads.

Many different constitutive equations for the strain rate behaviour of materials can be found in the literature. These equations contain empirical coefficients which have to be obtain by careful experiments. In this study the constitutive equation of Cowper and Symonds will be used, because it place relatively small demands on experiments, but give reasonable agreement with the available experimental data in the literature, see figure 4.3.

Cowper and Symonds come up with the constitutive equation written below [9].

$$\dot{\varepsilon} = D\left(\frac{\sigma_d}{\sigma_s} - 1\right)^q, \qquad \sigma_d \geq \sigma_s \tag{4.1}$$

where σ_d is the dynamic flow stress at an uniaxial plastic strain rate $\dot{\varepsilon}$, σ_s is the associated static flow stress and D and q are material dependent constants. Equation 4.1 can be rewritten as:

$$\sigma_d = \sigma_s\left(1 + \frac{\dot{\varepsilon}}{D}\right)^{\frac{1}{q}} \tag{4.2}$$

Now with use of this equation the dynamic flow stress can be obtain if the other values are known. Table 4.1 shows the coefficients D and q for various materials. A relation between a range of strain rates and the ratio between dynamic and static flow stress for those materials is plotted in figure 4.2. It can be seen that the dynamic flow stress is more sensitive to very high strain rates. Furthermore, the plot shows that mild steel is more sensitive for high strain rates, which happens to be the most common material used in construction. For further analysis the coefficients of mild steel will be used.

TABLE 4.1: Coefficients for various materials.[9]

Material	D (s^-1)	q	Reference
Mild steel	40,4	5	Cowper and Symonds
Stainless steel	100	10	Forrestal and Sagartz
High tensile steel	3200	5	Paik and Chung
Aluminium alloy	6500	4	Bodner and Symonds

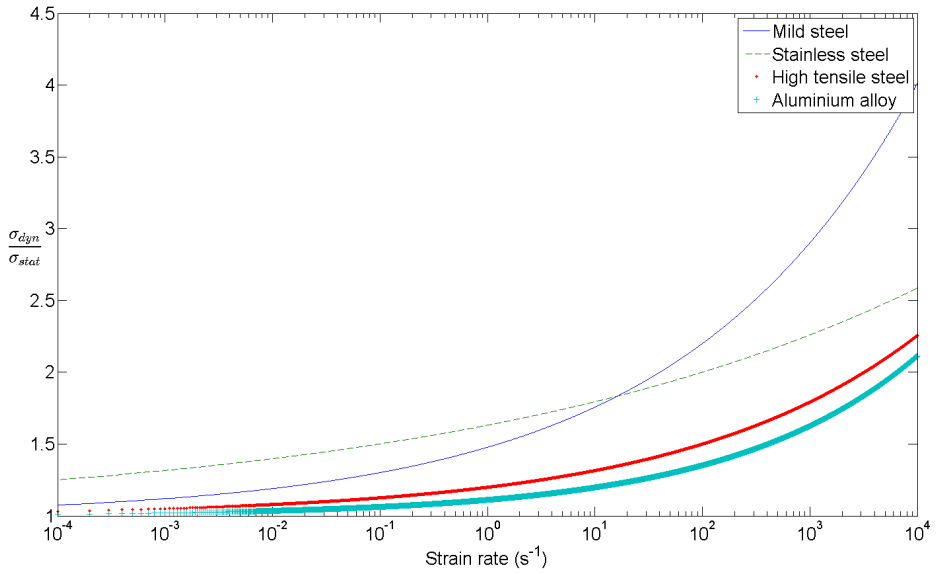

FIGURE 4.2: Behaviour of various materials according to Cowper and Symonds equation.

Looking at figure 4.3, where the experimental data obtained by several researchers shows that the equation 4.1 and 4.2 of Cowper and Symonds provides, from an engineering viewpoint, a reasonable estimation of the strain sensitivity behaviour of mild steel.

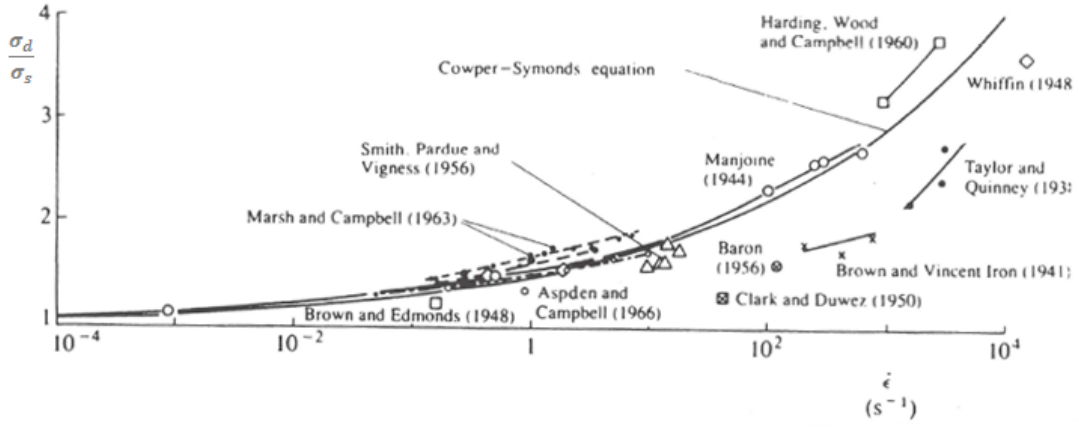

FIGURE 4.3: Variation of dynamic uniaxial lower yield stress of mild steel with strain rates. [14]

4.1 Procedure

The notion is to come up with factors to incorporate in preliminary calculations regardless of the structural arrangements and geometry. This is attempted by incorporating the strain rate sensitivity of the steel in preliminary calculations. In order to make use of the strain rate sensitivity, the strain rates occurring during the blast load has to be determined. A real experiment with explosives is not performed so another approach is chosen. The idea is to model structures in SACS and run a non linear plastic analysis to extract the strains occurring according to the software. Hereafter the strains will be differentiated to obtain the strain rates. A simple supported structure as seen in figure 4.4 is modelled in SACS for four different stiffness-weight combinations (theoretical dimensions) to check whether strain rate a geometry dependent phenomenon is or not, see table 4.2. The length of the beam, l is chosen to be 18 meters. A static load of 110 kN/m is applied exclusive the load of self-weight.

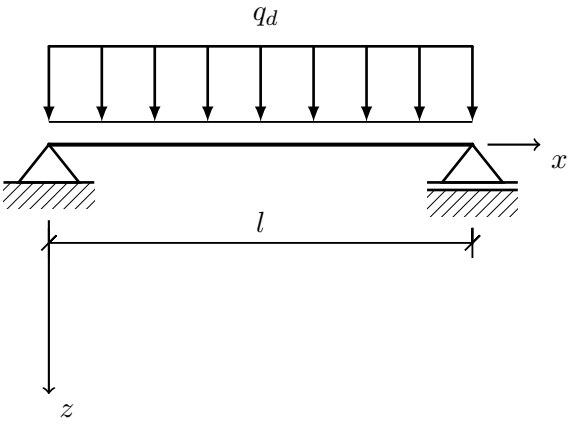

FIGURE 4.4: Simple structure with blast load.

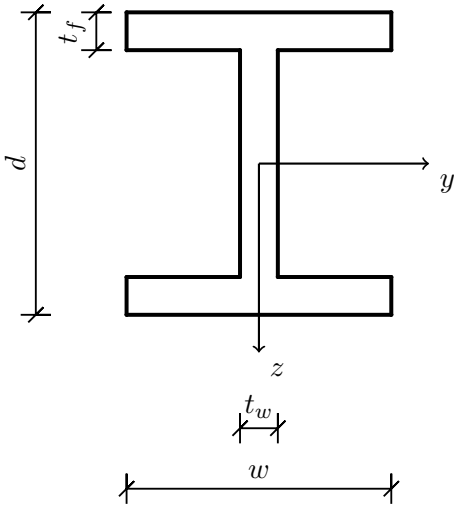

FIGURE 4.5: Symmetric plate girder.

TABLE 4.2: Dimensions of plate girder profiles

	width $w\ (cm)$	flange thickness $t_f\ (cm)$	height $d\ (cm)$	web thickness $t_w\ (cm)$	bending stiffness $EI_{zz}\ (MNm^2)$	weight (kg/m)
Stiff-Light	48	2	155	3,1	4227,6	518,2
Stiff-Heavy	70	12	80	5,8	4299,0	1573,8
Soft-Light	60	2,5	85	4,7	1493,4	530,7
Soft-Heavy	70	12	50	12	1352,9	1563,7

The primary beams in offshore topside structure are generally plate girders and to change beam profiles instead of the dimensions for the plate girder would be less convenient. As one can see in the table the dimensions for the plate girder are chosen in such a way that

the bending stiffness of a relative stiff plate girder is three times higher than a softer one. This ratio is also applied for the weight of the plate girder.

Four cases of blast load, q_d per girder profile are analysed to have at least one case where the structure is still intact and one case where the structure collapses. This is done to find out whether the collapse influences the strain rates. The elasticity with strain hardening stress-strain relation in figure 3.1c is used in SACS for this analysis.

The required input files for the Collapse analysis consist (see Appendix A of model file, file for determining the dynamic characteristics, collapse file and a force-time history file. The mesh length is again one meter, the fixity of the left support is 111101 (see Appendix A) and the right support with free horizontal movement is 011101. The fixity of the other point are 212000. The number of modes is in general for all files close to the maximum or where mass participation more than 98% is achieved. Furthermore, parameters in the Collapse file is the same as in table 3.2 of the previous paragraph. The Dynamic Response input file consist of values corresponding to the shape of the blast profile as mentioned in chapter 2 in figure 2.10, but with changing values for the positive peak pressure and the negative peak pressure depending on the blast scenario.

The strain reports from SACS for the corresponding profiles and load scenarios are exported and further processed in Matlab. Afterwards a strain-time graph is plotted to display the strain progression in time. The strain values are reported at each load step, which corresponds to the time interval of 0,005 seconds indicated in the Collapse input file. Differentiating the strain in time results in the strain rate of each sub segment. The strain rate of each segment is only taken when the strain value of that time did not exceed the elastic strain. In other words the strain rate of only the elastic part of the stress-strain diagram shown in figure 3.1c is considered. The reasons are because the equation 4.2 for determining the dynamic flow stress is not valid for high strains, the implementation to linear calculation is justified and the the material modelling are not properly customizable in the software which could lead pore strain registration after yielding, so the strain rates of only the linear part is derived.

4.2 Results

The strain-time and strain rate-time graphs are shown in figures 4.6 and 4.7 respectively. The values corresponds to the maximum strain of each segment of an element. The load on the structure in figure 4.4 results is no axial force, which means that the maximum strain is at the top and bottom of the flange, but with a different sign. The preferred way of obtaining strain reports from the software would be if the user could assign the

wanted areas in the cross section, however this is not possible. SACS gives the maximum positive or negative strain in the cross section as output. The maximum value (whether it is negative or positive) changes sometimes abrupt from sign after a load step, which is physically not possible to have a jump from tension to compression in that time frame. This occurs probably due to numerical errors, which causes for example the maximum strain at the top flange to be slightly smaller than the bottom in terms of absolute values. Since SACS reports the highest or lowest strain of that cross section a jump in the registered area seems to happen. For example in the previous load step it reports the strain value at the bottom flange which corresponds to tension and in the next load step it reports the top flange strain which corresponds to compression and hence the sign change. This problem will lead to higher strain rates, since the difference between the load steps will be much higher due to the sign change. To overcome this problem the absolute value of strain is taken and the reason why the graph shown in 4.6 is only positive. The blast loading displayed at the top of each cases should be read as follows: the first value is the peak positive value of the blast profile and the second value is the negative peak value, see figure 2.10. These loads represent the dynamic loads applied on the structure. The plots that do not reach the end time of 4 seconds are collapsed structures. Those are in general the ones with high strain rates. The absolute values of the strain rates are plotted, since the interest lies in finding the magnitude of the strain rate. What can be seen is that the strain rates of collapse are in the same order for the different cases. This shows that the geometrical differences does not have an effect on the maximum strain rates. A frame with bracing, see figure 4.9 is analysed the same way as the previous structure and this structure showed also strain rates similar to the simple structures. Thus the maximum strain rate, which happens when plasticity is achieved, seems to be independent of structure type.

Table 4.3 shows the maximum strain rate for each case and also the dynamic flow stress obtained by entering this strain rate in equation4.2. The coefficients D and q for mild steel are used and the applied static flow stress is $460\,N/mm^2$. The red cells represents the cases where the structure collapsed.

TABLE 4.3: Dynamic flow stress corresponding to obtained strain rates.

Case	Blast load (kN/m)	Max. strain rate (s^-1)	Dynamic flow stress (N/mm^2)	Ratio to yield stress
Soft-Heavy	$+60; -20$	$4,498 \cdot 10^{-3}$	534	1,16
	$+270; -90$	$1,327 \cdot 10^{-2}$	552	1,20
	$+330; -110$	$1,636 \cdot 10^{-2}$	556	1,21
	$+900; -300$	$3,334 \cdot 10^{-2}$	571	1,24
Soft-Light	$+60; -20$	$1,027 \cdot 10^{-2}$	548	1,19
	$+270; -90$	$2,111 \cdot 10^{-2}$	561	1,22
	$+330; -110$	$2,229 \cdot 10^{-2}$	563	1,22
	$+900; -300$	$3,551 \cdot 10^{-2}$	573	1,24
Stiff-Heavy	$+60; -20$	$5,163 \cdot 10^{-3}$	537	1,17
	$+270; -90$	$2,324 \cdot 10^{-2}$	563	1,22
	$+330; -110$	$2,840 \cdot 10^{-2}$	568	1,23
	$+900; -300$	$3,692 \cdot 10^{-2}$	573	1,25
Stiff-Light	$+60; -20$	$1,180 \cdot 10^{-2}$	550	1,20
	$+270; -90$	$4,207 \cdot 10^{-2}$	576	1,25
	$+330; -110$	$2,840 \cdot 10^{-2}$	568	1,23
	$+900; -300$	$4,660 \cdot 10^{-2}$	579	1,26
Braced Frame	$+60; -20$	$7,154 \cdot 10^{-2}$	542	1,18
	$+900; -300$	$5,338 \cdot 10^{-2}$	582	1,27

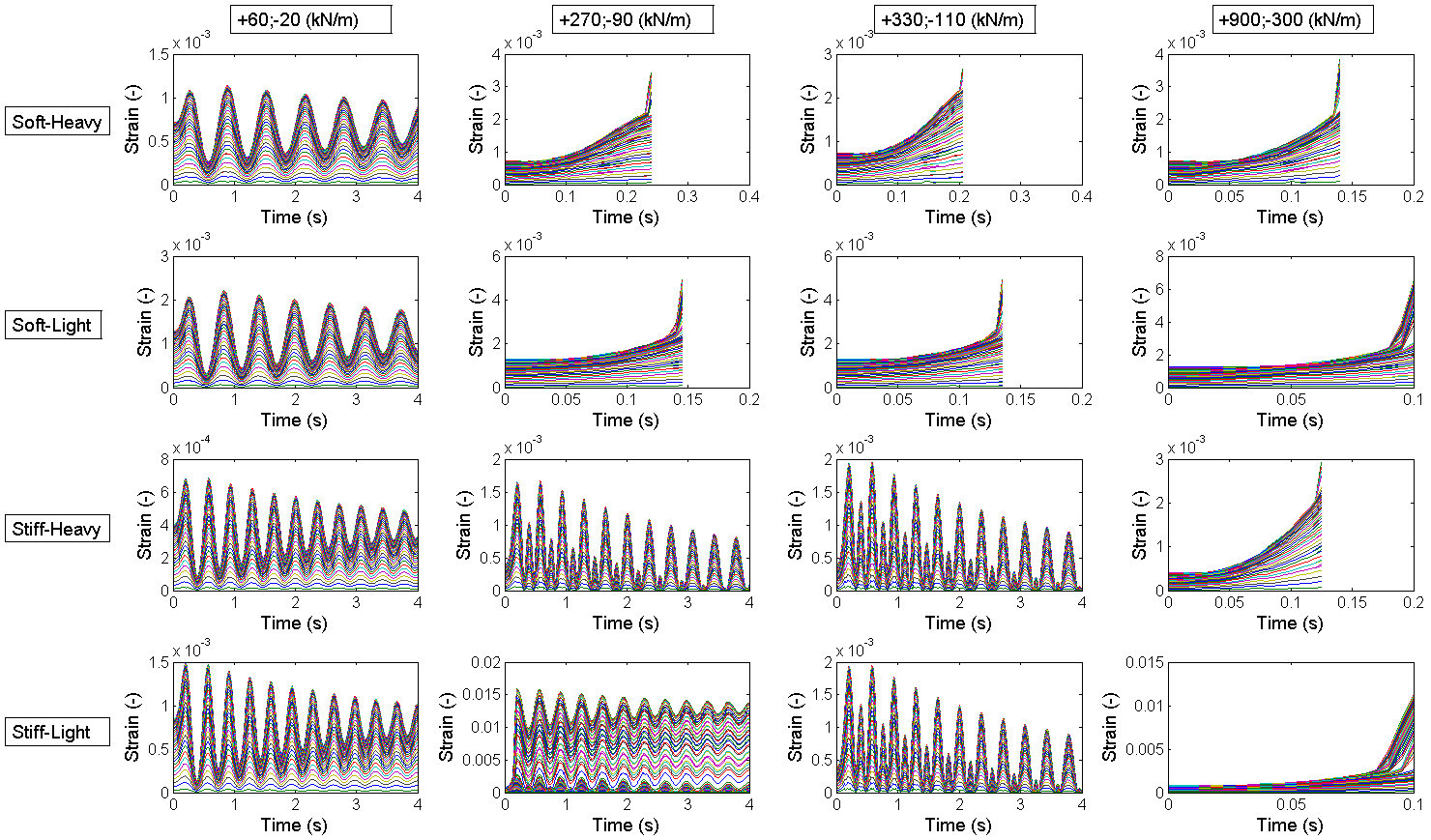

FIGURE 4.6: Strain-time graphs for four blast cases and profiles.(Absolute values of strains)

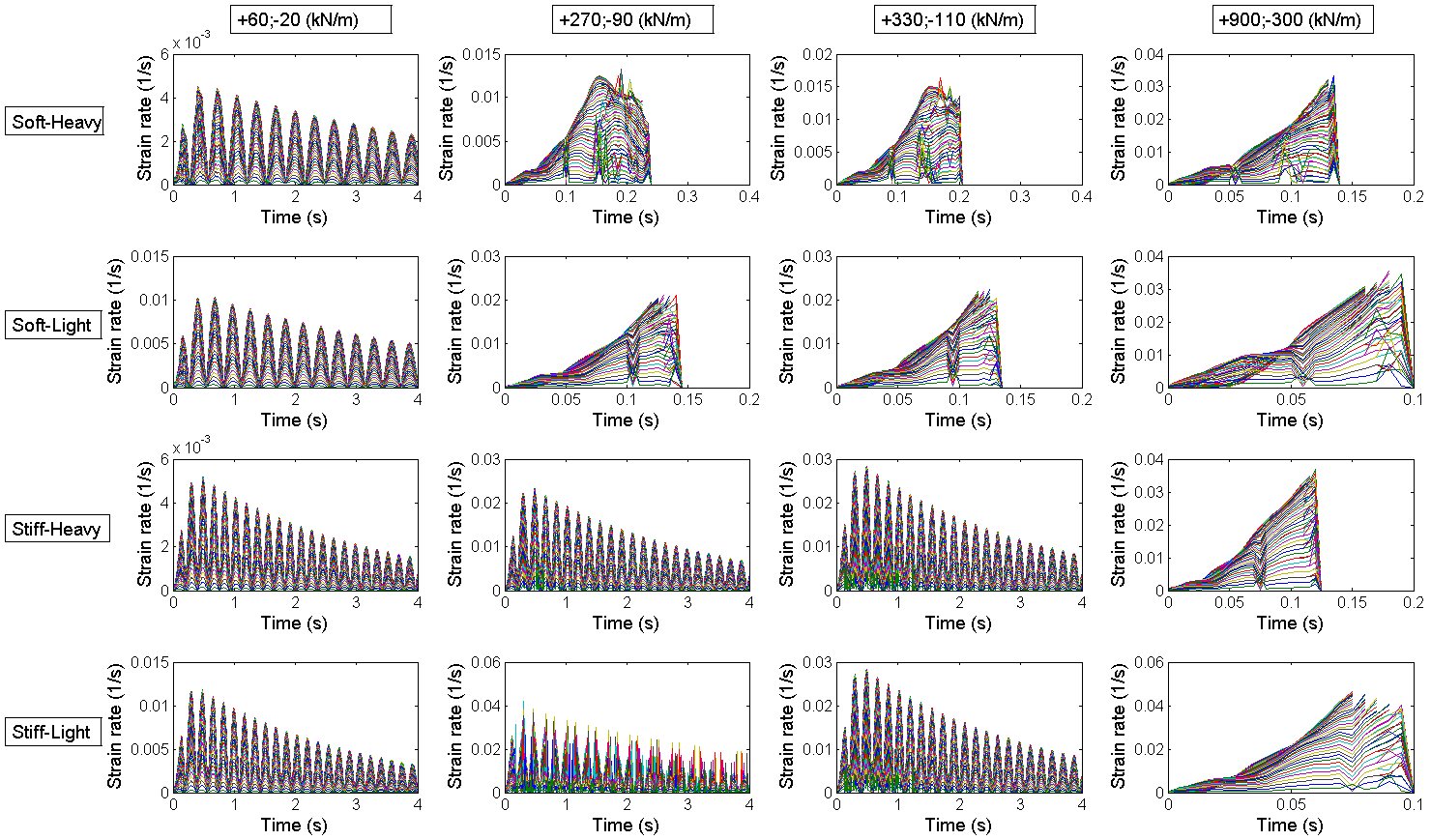

FIGURE 4.7: Strain rate-time graphs for four blast cases and profiles. (Absolute values of strain rates)

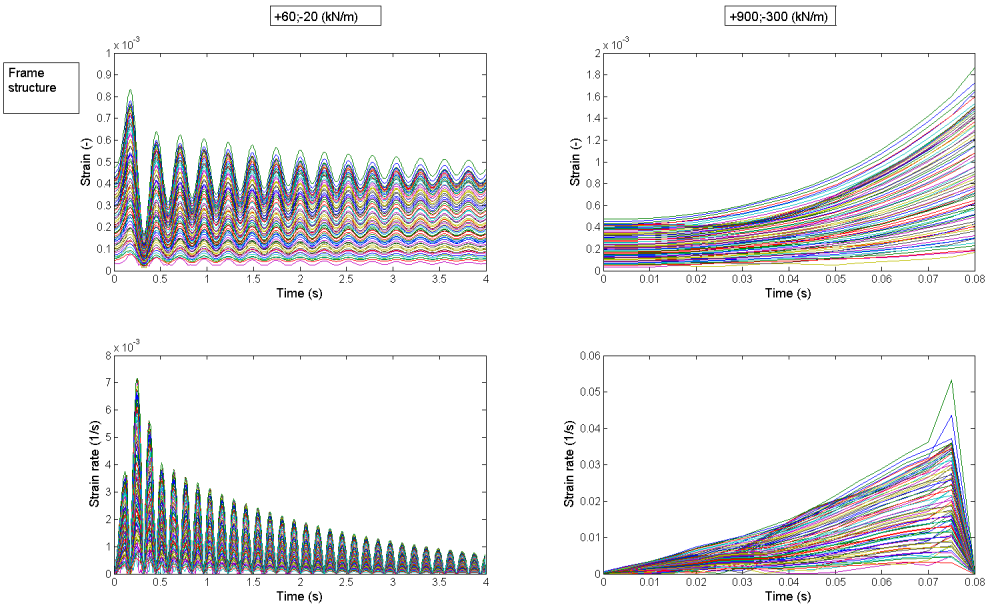

FIGURE 4.8: Strain-time and strain rate-time graphs for two blast loads for the braced structure.

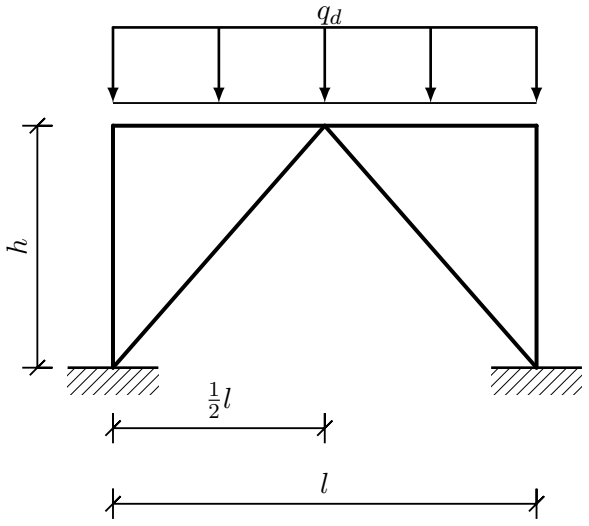

FIGURE 4.9: Braced structure

The load on top of the graphs shows the load factor of the positive and negative peak of the blast load. Each line represents a segment of an element. It can be seen that for some cases the structure collapses, hence the high strain. When the graphs of the strain rates are analysed one can see that the strain rates are much higher for structure that collapses, but for all collapsed structures the strain rate for the different stiffness weight ratios is in same order. This indicates that strain rate effect is independent of the structural geometry. A different system is chosen and compared to these results for

extra verification. The structure is shown in figure 4.9. The analysis is done the same except the vertical and diagonal columns are tubular and the support fixity is different. The results in SACS shows that this structure is more rigid, but the strain rate is also in the same order as the previous structure. This confirms that strain rate sensitivity, when plasticity is achieved, is independent of the structure geometry.

For the given strain rate of each structure with different blast loading a dynamic flow stress is calculated with the Cowper-Symonds equation. Table 4.3 shows the dynamic flow stress. The results shows reasonable consistency, for the collapsed cases, in terms of maximum strain rate. If one look for the maximum strain rates for each case it happens when the structure collapses and the corresponding dynamic flow stress is between 20% and 27% higher than the yield stress.

Based on these results, it is investigated whether a simplification could be made by changing the material model of strain hardening into elasticity with perfect plasticity including the dynamic flow stress act as a new yield stress. The maximum of the dynamic flow stress of each case is used as a yield stress input in Collapse software for the same structures to determine whether the result are the same when the absorbed energy by the stress strain curve is kept the same by changing ductility, see figure 4.10. The ductility changes for each dynamic flow stress in order to keep the absorbed energy equal, but it is for all the cases around 10,5%.

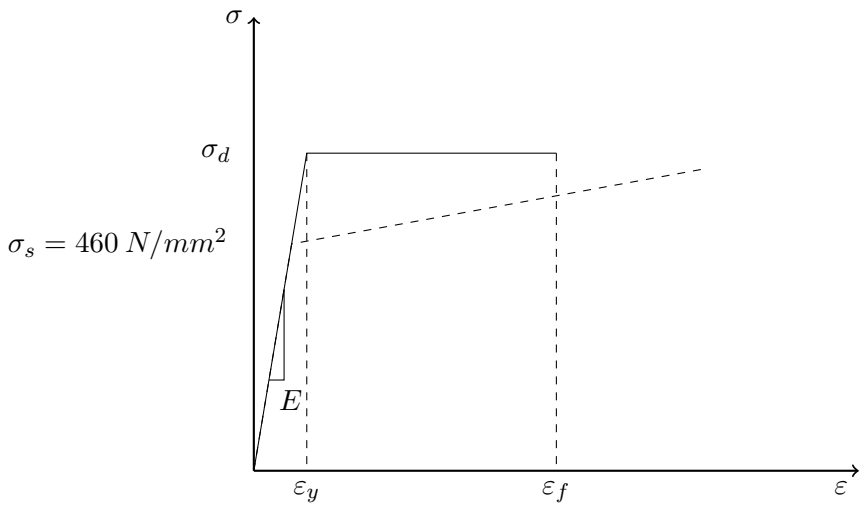

FIGURE 4.10: New stress-strain relation used in SACS for comparison

Calculating the structures with the new ductility and yield stress for the same blast loads resulted in not collapsing of the Soft-Heavy $+270; -90$ and $+330; -110$ and the same with Stiff-Light $+330; -110$. This means that even when the absorbed energy is kept the same the results differs. Thus, the yield stress replaced by the dynamic flow stress results in a structures with a higher load bearing capacity, even when the toughness

is kept the same. There are big gaps between the loads of the applied load cases so how much increase is took place is not determined yet. The Soft-Heavy case is further analysed in order to determine the increase in load bearing capacity between the two material models. First the lower bound of collapse load is determined for the original stress strain curve and then the upper bound of collapse load is determined for the adapted stress strain curve. After an iterative procedure it was found that the structure can withstand a maximum blast load of $+210; -70\ kN/m$ for the initial stress strain curve and the maximum blast load for the structure with stress strain curve based on the dynamic flow stress is $+450; -150\ kN/m$. Based on this result it can be concluded that at least by using this method an increase of 114% is seen. Therefore, it can be concluded that keeping the toughness the same, but changing the yield stress and ductility leads to different result. It is shown that a material model with a higher yield stress and lower ductility results in a stronger structures than a material model with a lower yield stress and higher ductility. This is also seen when the ductility is reduced (also fracture energy) to proportionality limit, which is still stronger than the original material model with yield stress of 460 N/mmm^2 and 12% ductility with strain hardening.

To conclude, in table 4.3 is dynamic flow stress given for the corresponding strain rate. At least an increase of 20% in yield stress for a blast load is seen. This means that for a blast analysis the initial yield stress ($460\,N/mm^2$) of an elastic calculations can be increased to approximately 20% ($552\,N/mm^2$). This can easily be modified in the post processing of SACS.

Chapter 5

Conclusion and discussion

In this thesis an elastic and plastic blast analysis has been executed in order to compare the results and determine the exceedance that could be allowed in linear calculations. Furthermore the influence of strain rate is presented and included in linear calculations. Based on this analysis several conclusions have been drawn and some discussion points and recommendations are provided, which are listed below.

5.1 Conclusions

- For the structure in paragraph 3,2 was shown that the static distributed load bearing capacity is increased by 1,11k when plasticity is allowed. Depending on the shape of the plate girder the total increase is near 30% compared to linear calculations. This increase factor is also depending on the ratio between the height and length of the structure and the stiffness ratio between the plate girder and column.
- The number of member segments specified in the Collapse input file for a plastic analysis has to be 4 or more to predict a hinge accurately. Obviously more member segments are better, but the number has a big impact on the computation time, which can play a big role in complete topside analysis.
- The tolerance in the Collapse input file needs to be set properly. In the static plastic analysis the software uses iterations in each load step. In these iterations the node displacement and node rotations are improved until al equations are fulfilled to sufficient degree of accuracy. the required accuracy of tolerance is input as a node displacement difference between two subsequently iteration or a node rotation difference between two subsequent iterations. During multiple calculations was found that the load bearing capacity was 50% overestimated.

- The results of the dynamic analysis for different cases showed that when the column is stiff compared to the beam ($\frac{EI_b}{EI_c} < 1$) the stresses are more concentrated at the side of the beam and when the beam is more stiff compared to the column ($\frac{EI_b}{EI_c} > 1$) the difference between the stress at the side of the beam and midspan becomes smaller. And regarding case 5 where the structures collapses the right column and midspan have a higher stress compared to the left side. This can also be seen for the lower graph where the size of the beam is changing, except the stress for ($\frac{EI_b}{EI_c} < 1$) is too high and the structure collapses. But the same phenomenon is taken place. So when the bending stiffness of the column is decreasing then this leads to the redistribution of the stresses from the lefts side of the beam to the midspan.

- The graphs showed that the stresses for elastic and plastic analysis are the same for cases where the structure did not collapse (1, 2, 3, 4, 7 and 8). For case 5 the left side of beam and the right upper column side shows 20% more stress for elastic analysis compared to plastic analysis and 11% increased stress for the midspan for plastic analysis compared to elastic. This means that when plasticity is allowed, then the stresses are redistributed to the midspan leading to an increase of stress there and decrease of stress at the side of the beam. For case 6 (bottom graph) the plastic analysis shows approximately 7% increase in stress for the left side of the beam compared to elastic analysis. For the midspan there is only 4% difference between plastic and elastic analysis.

- When the UC is high than 1 and nowhere in the structure appears a stress above the yield stress then during a plastic analysis the structure will remain intact. The high UC is then caused by a low allowable stress due to the slenderness of the plate girder and/or reductions implemented by design codes.

- An UC of 1,14 in an elastic dynamic analysis can already lead to collapse in a plastic dynamic analysis. However, once an UC of 2,75 in an elastic dynamic analysis did not lead to collapse in a plastic dynamic analysis. Therefore it can be concluded that the rule that an UC of 1,30 is acceptable is neither economical nor always safe and therefore a generalisation of 30% increase in UC should not be used, but has to be decided for each situation.

- For different stiffness-weight combination is found that the maximum strain rate for the elastic part of the material model arises at the transition between the elastic and plastic part. When this strain rate is compared between the different cases it was found that the geometry does not influence the strain rate when the structure collapses due to the load.

- Based on the used blast profiles the obtained strain rates resulted in a dynamic flow stress that is compared to the yield stress 20% to 27% higher. Thus, in the early design phase the yield stress of the material can be increase by this percentage for a blast load.
- The two material models with the same toughness, different yield stress and ductility showed in one case a difference of 114% in resisting blast load. The material model with a relative high yield stress and low ductility leads to a stronger structure.
- To conclude, the dynamic flow stress for the corresponding strain rates showed an increase of at least 20% for the collapsed structures. This means that for a blast analysis the initial yield stress ($460\,N/mm^2$) of an elastic calculations can be increased to approximately 20% ($552\,N/mm^2$).

5.2 Discussion and Recommendation

- A detonation type of explosion is not taken into account which could happen when there is confinement and blockage due to equipments en piping. The arising pressure will be higher and more detrimental for the topside. Also, reflection of the pressure is not taken into consideration. This could lead to inaccurate design load.
- It was shown that the geometry and blast load does not influence the strain rate, however the strain rate is influenced by the duration of the blast pressure. This is the main contributor for the different progression in strain rate. The impulse durations are close to each other. Even if the duration is changed for a blast analysis the occurring strain rate is in the same order of magnitude and since the dynamic flow stress is not sensitive for strain rate values in the same order the results will not differ to much.
- The strain progression in time are extracted from SACS and thus the strain rate, but an experimental study would increase the reliability of this analysis.
- The modelling of the structures were al in 2D this means the pressure is converted to a distributed load which is assumed to be equally distributed along the length to the beam. However the phase difference can increase the impact of the blast load. It is also assumed that the plating on the deck is not collapsing and transferring the loads to the plate girder.
- The gain by the strain rate sensitivity can be used in the early design phase for the linear analysis, however when non linear analysis is performed later on, the

software will not take this effect into account. So it may report that the structure is collapsing, when in reality it is not necessarily true. The maximum dynamic load on a structure could just stay beneath the maximum dynamic flow stress and not exceed the elastic strain limit. Thus, the results of the software will be more conservative. Also, a factor for increasing the material strength of a structure during design may seem to be counter intuitive, but the structure is not expected to experience several blast loads during the lifetime.

- The influence of heat is not taken into account. A structure becomes less strong when a fire accident is taken place and if this accident is followed up by an explosion then the structure will lose significant amount of strength. A study of a structure subjected to high temperatures combined with a blast load is recommended.

- It is also recommended that a simple non linear analytic analysis should be performed to verify the dynamic plastic SACS results in terms of the tolerances in input file. It was shown in the static plastic analysis that the tolerance set in the Collapse input file was sensitive and not straight forward leading to large deviation in accuracy when it was not set properly.

- Furthermore, a study for a blast absorbing structural element would be recommended in order to absorb a portion of the blast load to reduce to loading on the main structural elements.

Bibliography

[1] *NORSOK Standard Z-013*, 3 edition, October 2010. Annex F: Procedure for probabilistic explosion simulation.

[2] *SACS- Precede, Dynpac, Dynamic Response, Collapse, Combine Postvue*, 7.0 edition, 2012.

[3] A. Bakri and A. J. Watson. Factors affecting a rc slab response to blast loading. In *Asia-Pacific Conference on Shock and impact loads on structures*, pages 11 – 18, 1996.

[4] Tormod Bjontegaard. Probabilistic explosion analysis of aasta hansteen. Technical report, Scandpower AS, 2014.

[5] John M. Dewey. The shape of the blast wave: studies of the friedlander equation. 1741 Feltham Road, Victoria, BC V8N 2A4, Canada, 2010.

[6] Committee for the Prevention of Disasters. *Methods for the determination of possible damage to people and objects resulting from releases of hazardous materials, CPR 16E.* Publication Series on Dangerous Substances. The Dutch Ministry of the Interior and Kingdom Relations, The Hague, The Netherlands, first edition, 1992. Green Book, 2005 revision of the first edition published in 1992.

[7] F. G. Friedlander. The diffraction of sound pulses. i. diffraction by a semi-infinite plane. *Proceedings of the Royal Society of London. Series A, Mathematical and Physical Sciences*, 186(1006):322–344, 1946.

[8] T.C. Fung and S.K. Chow. Responses of blast loading by complex time step method. *Journal of Sound and Vibration*, 1999.

[9] Norman Jones. *Structural Impact.* Cambridge University Press, 1990.

[10] C. Leung and S. Mahajan. Topside structure blast analysis report. Technical report, CB&I, 2014.

[11] K.J. Marsh and J.D. Campbell. The effect of strain rate on the post-yield flow of mild steel. *Journal of the Mechanics and Physics of Solids*, 11, 1963.

[12] A.V. Metrikine. Dynamics, slender structures and an introduction to continuum mechanics: Ct 4145 lecture notes.

[13] James H. Stuhmiller, Yancy Y Phillips III, and Donald R. Richmond.

[14] P.S. Symonds. Survey on methods of analysis for plastic deformations of structures under dynamic loading, 1967.

[15] A.C.W.M. Vrouwenvelder. The plastic behaviour and the calculation of beams and frames subjected to bending: Ct 4150 lecture notes, 2003.

[16] Lars Weie. Gas and smoke dispersion. Technical report, Scandpower AS, 2014.

Appendix A

SACS solution method

SACS is an integrate suite of software that supports the analysis, design and fabrication of offshore structures. The software consist of several program modules for different purposes. The following analysis are performed in this thesis static elastic analysis, static plastic analysis, dynamic elastic analysis and dynamic plastic analysis. Each module used for these analyses requires certain input file(s) and generates output file(s) which are then used for the next module(s). The required software modules in subsequent order for each type of analysis are:

- **Static elastic**: Precede
- **Static plastic**: Precede and Collapse
- **Dynamic elastic**: Precede, Dynpac, Dynamic response, Combine and Postvue
- **Dynamic plastic**: Precede, Dynpac and Collapse

The description and calculation methods for the following sections are to be found in the manuals of SACS [2]. The next sections summarizes the explanation of the relevant modules.

A.1 Precede

In this module the model is generated including geometry, material and section properties. The static loading is applied and the mass distributing of the model is defined by notation of nodes, which imply a certain property. The nodes property is given by the numbers 0, 1 and 2 which stands for free, fix and master joint respectively.

An example of a node notation is 012000. The first three numbers represent the displacement freedom in the x, y and z directions. The last three numbers represent the rotation freedom around the axis of x, y and z. In this example it is a simple support with free movement in x and z directions and fixed in y direction, where only the mass in z direction is participating and no restrains in rotation freedom around the three axis.

A.2 Dynpac

Dynpac is a linear dynamic analysis module that generates dynamic characteristics. It was used to determined the structural modes of vibration and to extract the modal shapes, mass and modal internal load and stress vectors for the structure. Dynpac uses the master degree of freedom, selected by user, to extract the eigen values and eigen vectors. All stiffness and mass properties associated with the slave degree of freedom are included in the eigen extraction procedure. The stiffness matrix is reduced to the master degrees of freedom using standard matrix condensation methods. The number of modes shapes chosen for the performed analyses in this thesis is such that there is at least 98% mass participation based on the degree of freedom.

A.3 Dynamic response

The dynamic response module computes the dynamic responses of a structure subjected to dynamic excitation due to base motion such as in an earthquake, dynamic forces due to periodic vibration or impact loads. The program can analyse base driven systems with input described either as a spectral input or as a time history input, and force driven systems with input described by a set of period forces or time history forces. In this thesis the dynamic response is a force driven system with time history force of the blast.

A.4 Combine

The combine module is an utility program. It allows the user to combine static and/or dynamic results of the same model from various analysis into a single solution file. The program has the ability to combine results from dissimilar post files allowing results of various construction stages to be interpreted.

A.5 Postvue

This program was developed to provide the user with an intuitive and efficient tool for reviewing, printing, and plotting analysis results, and redesigning structural members.

A.6 Collapse

The SACS module collapse is a large deflection, elasto-plastic, non linear finite element system for structures. The program is fully integrated into the SACS suite of programs and uses the same input data as that for a standard analysis. The software will divide the members in segments (finite elements) along the member length. For the static analysis the load is applied incrementally from 0% to 100% and the von Misses stress, strain and deflection are recorded for every finite element. Regarding a dynamic analysis (e.g force-time history) the same procedure is followed in each time interval. When a segment reaches elastic limit, the plastic behaviour is simulated, including the strain hardening. When the entire section is plastic, a plastic hinge is introduced at that location. The non linear effect due to large deflections will also be accounted in the analysis. SACS stops the analysis and reports collapse in the following cases. The structure is considered to be collapsed when a mechanism is formed, which is signified by a non-positive definite stiffness matrix. A mechanism takes place due to plastic hinges formation in the structure in combination with a disconnected member or by a disconnected member by itself. A member disconnects (ruptures) when the maximum allowed strain is exceeded. The structure is also considered to be collapsed when a very large displacement, defined by the user, occurs for a small increase in load. This deflection corresponds to the largest joint displacement in the whole model. The solution method used by collapse module is further explained in the following sections.

A.6.1 Energy principle

The energy, or variational methods of structural mechanics constitute a widely used approach. The following sections explains the basic energy variational principles used by the non linear Collapse module. This explanation originated from SACS manual [2].

A.6.2 Discrete systems

In a discrete system the potential energy, V can be expressed as a function of displacements q_i and loads P_i. The potential energy of the system, considering small variation

in displacements δq_i, can be expressed assuming load P_i remains constant via a Taylor's series expansions as:

$$V(P_i, q_i + \delta q_i) = V(P_i, q_i) + \frac{\partial}{\partial q_i} V(P_i, q_i)\delta q_i + \frac{1}{2!}\frac{\partial^2}{\partial q_i \partial q_j} V(P_i, q_i)\delta q_i \delta q_j + ... \quad \text{(A.1)}$$

This equation can be written as:

$$\delta^T V = \delta V + \delta^2 V + ... \quad \text{(A.2)}$$

where the total variation in the potential energy, $\delta^T V$ is described as:

$$\delta^T V = V(P_i, q_i + \delta q_i) - V(P_i, q_i) \quad \text{(A.3)}$$

where δV and $\delta^2 V$ are the first and second variations of the potential energies given by:

$$\delta V = \frac{\partial}{\partial q_i} V(P_i, q_i)\delta q_i \quad \text{(A.4)}$$

and

$$\delta^2 V = \frac{1}{2!}\frac{\partial^2}{\partial q_i \partial q_j} V(P_i, q_i)\delta q_i \delta q_j \quad \text{(A.5)}$$

A.6.2.1 Discrete system-equilibrium

In order to achieve equilibrium for the system, the potential energy has to be stationary with respect to displacements so that for all admissible values of δq_i, the first variation of the total potential energy is zero, i.e.:

$$\delta V = \frac{\partial}{\partial q_i} V(P_i, q_i)\delta q_i = 0 \quad \text{(A.6)}$$

For $i = 1...n$, equation A.6 yields n equilibrium equations. Considering an equilibrium system so that δV=0, equation A.2 can be rewritten as:

$$\delta^T V = \delta^2 V + ... \quad \text{(A.7)}$$

A.6.2.2 Discrete system-unstable equilibrium

If the system in its new configuration, $V(P_i, q_i + \delta q_i)$ is in a state of stable equilibrium, then the total variation in potential energy, $\delta^T V$, is a minimum and the second variation is $\delta^2 V$ is a quadratic form in δq_i and is positive definite for all admissible values of δq_i. When $\delta^2 V$ changes from positive definite to semi-positive definite the condition will

be unstable or critical. This indicates a possible transition from stable to unstable equilibrium.

A.6.2.3 Discrete system-non linear problems

For non linear problems, the first variation of the potential energy, δV, yields n unknown non linear equations in the displacement variables $q_i (i = 1...n)$. If Δ represents a small but finite increment in displacements and forces, then the first variation of the potential energy $\delta V(P_i + \Delta P_i, q_i + \Delta q_i)$ can be expanded in a Taylor series about the (P_i, q_i) configuration yields:

$$\delta V(P_i + \Delta P_i, q_i + \Delta q_i) = \delta V(P_i, q_i) + \frac{\partial}{\partial P_i} V(P_i, q_i)\Delta P_i + \frac{\partial}{\partial q_i} V(P_i, q_i)\Delta q_i + ... \quad \text{(A.8)}$$

After rearranging equation A.8 and keeping only first order terms in increments Δ yields:

$$\delta V(P_i + \Delta P_i, q_i + \Delta q_i) - \delta V(P_i, q_i) = \frac{\partial}{\partial P_i} V(P_i, q_i)\Delta P_i + \frac{\partial}{\partial q_i} V(P_i, q_i)\Delta q_i + ... \quad \text{(A.9)}$$

If the system in configuration $(P_i + \Delta P_i, q_i + \Delta q_i)$ is in equilibrium then:

$$\delta V(P_i + \Delta P_i, q_i + \Delta q_i) = 0 \quad \text{(A.10)}$$

Substituting equation A.10 into equation A.9, rearranging the terms and ignoring higher order terms yields the following equation:

$$\frac{\partial}{\partial q_i} V(P_i, q_i)\Delta q_i = -\frac{\partial}{\partial P_i} V(P_i, q_i)\Delta P_i - \delta V(P_i, q_i) \quad \text{(A.11)}$$

Equation A.11 provides a basis for an iterative procedure for the solution of non linear equilibrium equations and when $\delta V(P_i, q_i)$ is set to zero the equation represents the incremental equation of equilibrium.

A.6.3 Continuous systems

The variational principles for discreet systems can also be used for continuous systems.The loads P_i and displacements q_i in the discrete system can be assumed similar to the externally applied loads and nodal displacement coefficients which defines the magnitude of displacements in continuous systems.

A.6.3.1 Continuous systems-equilibrium

Consider a system consist of a deformable body with external forces P_i with the corresponding displacements defined by r_i. The system is in a state of equilibrium when the first variation of the potential energy is zero. When the external forces are assumed to remain constant then the first variation of the potential energy is represented by the following equation:

$$\delta V = -P_i \delta r_i + \int \sigma_i \delta \varepsilon_i dVOL = 0 \tag{A.12}$$

where the index i imply summation, σ_i represents the internal stresses, $\delta\varepsilon_i$ represents the first variation in the corresponding strains and the integration is over the volume of the body. The second variation of V, $\delta^2 V = \delta(\delta V)$, is given as:

$$\int (\sigma' \delta \varepsilon_i + \sigma_i \delta \varepsilon_i') dVOL = P_i' \delta r_i + P_i \delta r_i - \int \sigma_i \delta \varepsilon_i dVOL \tag{A.13}$$

A.6.3.2 Continuous systems-unstable equilibrium

A stable equilibrium for a continuous system is similar to discrete system, so the first variation corresponds to a minimum and is zero and the second variation is positive definite for all variations in displacements. As mentioned before the conditions becomes unstable or critical when $\delta^2 V$ changes from positive definite to semi-positive definite. In order to completely define equation A.13 it is necessary to consider second order strains and displacements, because the second variation of any linear function vanishes.

A.6.3.3 Continuous systems-non linear problems

Assuming that r_i can be expressed as a linear function of displacement variables and σ_i and ε_i can be expressed as functions of displacement variables, equation A.11 and equation A.12 yield:

$$\int (\sigma_i' \delta \varepsilon_i + \sigma_i \delta \varepsilon_i') dVOL = P_i' \delta r_i + P_i \delta r_i - \int \sigma_i \delta \varepsilon_i dVOL \tag{A.14}$$

in which the prime implies the operation

$$\frac{\partial f(x)}{\partial x_i} \Delta x_i$$

with respect to the applied load and displacement variables.A basis for an iterative procedure for the analysis of non linear equilibrium equations is provided by equation A.14, which is similar to equation A.11 for a discrete system. Equation A.14 represents

the incremental equations of the equilibrium when the last two terms on the right hand side of the equation are set to zero.

A.6.4 Non linear plastic force approach

For an elasto-plastic problem, the strains can be expressed in terms of the displacement variables in matrix form as:

$$\{\varepsilon_i\} = \big[A\big]\{q\} \tag{A.15}$$

where ε_i is the total strain vector at a point and can be described as the elastic strains $\varepsilon_{e,i}$ plus the plastic strains $\varepsilon_{p,i}$ so that:

$$\{\varepsilon_i\} = \{\varepsilon_{e,i}\} + \{\varepsilon_{p,i}\} \tag{A.16}$$

Stresses σ_i which are only dependent on elastic strains can be expressed as:

$$\{\sigma_i\} = \big[E\big] + \{\varepsilon_{e,i}\} \tag{A.17}$$

Noting that:

$$\{\sigma_i'\} = \big[E\big] + \{\varepsilon_i'\} \tag{A.18}$$

and substituting the equations A.16 - A.18 into equation A.14 gives:

$$\begin{aligned}\int \Big(\Big[\{\delta q\}^T \big[A\big]^T - \{\delta\varepsilon_p\}^T\Big] \big[E\big] \Big[\big[A\big]\{\Delta q\} - \{\varepsilon_p'\}\Big] + \\ \big[E\big]\Big[\big[A\big]\{q\} - \{\varepsilon_p\}\Big]\Big) dVOL = \{\delta q\}^T\{\Delta P\} + \{\delta q\}^T\{P\} - \\ \int \Big(\Big[\{\delta q\}^T \big[A\big]^T - \{\delta\varepsilon_p\}^T\Big] \big[E\big] \Big[\big[A\big]\{q\} - \{\varepsilon_p\}\Big]\Big) dVOL\end{aligned} \tag{A.19}$$

where

$$\{P\} = \{P_a\} + \{P_p\} \tag{A.20}$$

$$\{\Delta P\} = \{\Delta P_a\} + \{\Delta P_p\} \tag{A.21}$$

$\{P_a\}$ is the applied load vector and $\{P_p\}$ is the plastic load vector, $\{\Delta P_a\}$ and $\{\Delta P_p\}$ are the corresponding load increment vectors. Since the degree of plasticity incurred (and as a result the plastic load vector) is a function of the load path, the solution of an elasto-plastic problem must be handled on an incremental basis given by equation A.19 which represents a set of linear simultaneous equations in the unknowns $\{\Delta q\}$ and $\{\Delta P_p\}$. The solution procedure involves the application of a linear load increment $\{\Delta P\}$, and solving the equations for the unknown increments. The improved approximations of $q + \Delta q$ and $P + \Delta P$ are then used as a starting point for the next improvement cycle.

The procedure is continued until equilibrium is satisfied. This can be demonstrated by the vanishing of the last two terms on the right hand side of equation A.19.

A.6.5 Beam elements

A.6.5.1 Non linear strain expressions

The complete non linear expressions for the strains occurring in the tubular, wide flange, angles, channels and tee cross section types is given by the following equation:

$$\varepsilon_x = -y\left(\frac{d^2v}{dx^2} + \frac{d^2w}{dx^2}\theta\right) - z\left(\frac{d^2w}{dx^2} + \frac{d^2v}{dx^2}\theta\right) + \alpha_w\left(\frac{d^2\theta}{dx^2} - \frac{d^3w}{dx^3}\frac{dv}{dx} + \frac{d^3v}{dx^3}\frac{dw}{dx}\right) + \frac{du}{dx} + \frac{1}{2}\left(\frac{du}{dx}\right)^2 + \frac{1}{2}\left(\frac{dv}{dx}\right)^2 + \frac{1}{2}\left(\frac{dw}{dx}\right)^2 + \frac{\rho^2}{2}\left(\frac{d\theta}{dx}\right)^2 \tag{A.22}$$

The first two terms in the above equation represent the bending strains including the interaction between bending and twisting. The third term in the expression results from the restraint in warping. In practice, partial or no restraint in warping may exist and may differ for various structural connection types. Because of this, it is difficult to quantify and hence is not considered by the program. The terms on the last line of the equation represent strains produced by stretching of an element due to displacements u, v and w. The second order strain in u can also be neglected in the above equation since its contribution can be assumed to be small in comparison with other terms. Altogether the resulting strain expression becomes:

$$\varepsilon_x = -y\left(\frac{d^2v}{dx^2} + \frac{d^2w}{dx^2}\theta\right) - z\left(\frac{d^2w}{dx^2} + \frac{d^2v}{dx^2}\theta\right) + \frac{du}{dx} + \frac{1}{2}\left(\frac{dv}{dx}\right)^2 + \frac{1}{2}\left(\frac{dw}{dx}\right)^2 + \frac{\rho^2}{2}\left(\frac{d\theta}{dx}\right)^2 \tag{A.23}$$

The expression for shear strain due to St. Venant torsion is given by the following expression:

$$\varepsilon_{xy} = 2\xi\left(\frac{d\theta}{dx} - \frac{d^2w}{dx^2}\frac{dv}{dx} + \frac{d^2v}{dx^2}\frac{dw}{dx}\right) \tag{A.24}$$

When considering the effects of St. Venant torsion on thin walled bars of open cross section, the section can be considered to be composed of single or several disconnected rectangular strips.

A.6.5.2 Non linear Problems

The first variation of the total potential energy for a thin walled bar of open cross-section δV is formulated as:

$$\delta V = -P_i \delta r_i + \int \left(\sigma_x \delta\varepsilon_x + \sigma_{xy}\delta\varepsilon_{xy}\right) dVOL \tag{A.25}$$

where σ_x is the axial stress (tensile positive), $\delta\varepsilon_x$ is the first variation of the axial strains, ε_{xy} is the shear stress and $\delta\varepsilon_{xy}$ is the first variation in the corresponding strain. The relationship between the stresses and strains may described as:

$$\sigma_x = E\varepsilon_x \tag{A.26}$$

$$\sigma_{xy} = G\varepsilon_{xy} \tag{A.27}$$

where E is the Young's Modulus and G is the shear modulus. As written before, equation A.14 provides a basis for an iterative procedure to the solution of non linear equations. For a thin walled bar of open cross-section, equation A.14 can be rewritten as:

$$\begin{aligned} &\int \left(\sigma'_x \delta\varepsilon_x + \sigma'_{xy}\delta\varepsilon_{xy} + \sigma_x \delta\varepsilon'_x + \sigma_{xy}\delta\varepsilon'_{xy}\right) dVOL \\ &-P'_i \delta r_i = P_i \delta r_i + \int \left(\sigma_x \delta\varepsilon_x + \sigma_{xy}\delta\varepsilon_{xy}\right) dVOL \end{aligned} \tag{A.28}$$

Expressing stresses in terms of strains by using the strain expressions of equation A.23 and integrating over the volume of the bar, equation A.28 can be written in matrix form as:

$$\left[K_{inc}\right]\{\Delta q\} - \{\Delta P\} = \{P\} - \left\{K_e\right\}\{q\} \tag{A.29}$$

Equation A.29 represents a set of linear equations in the unknown displacement increments $\{\Delta q\}$ and load increments $\{\Delta P\}$, which can be solved iteratively. The left side of the equation describes the incremental equations of equilibrium and the right side describes the equilibrium equations. In a state of equilibrium the right hand side vanishes. The member element is divided along its length into sub-elements to account for the inter-nodal large displacement non linearities. The number of sub-elements is controlled by the user up to a maximum of twenty-four, with a default of eight. This subdivision will allow the program to account for inter-nodal buckling as well as predict the contribution of the inter-nodal large displacements on the surrounding structure. Each member that is sub-divided essentially becomes a super-element to the structure. From the global stiffness analysis, the member end deflections and rotations are known as well as any inter-nodal loading. Figure A.1 shows an example of the subdivision of one element in four sub-elements.

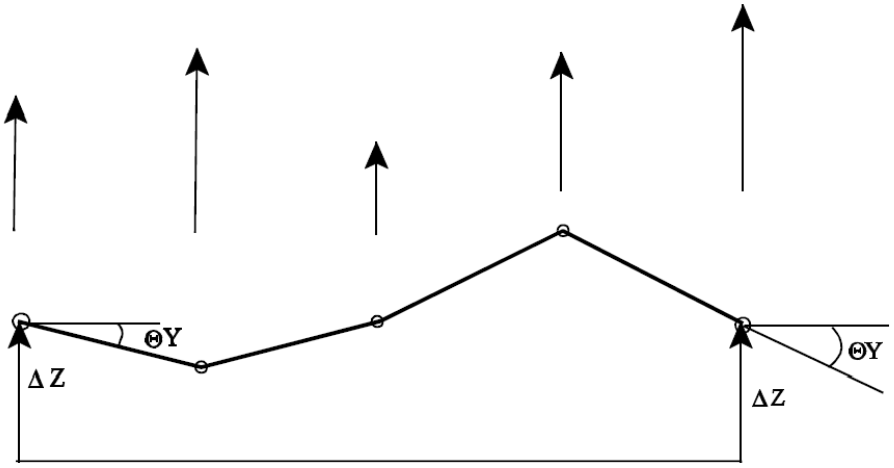

FIGURE A.1: Inter nodal loading. [2]

This super-element is solved iteratively using the end deflections and rotations and the intermediate loading until the internal deflections and rotations have converged. At each iteration, each sub-element is checked for plasticity as follows:

1. The internal loads at each end of the sub-element is calculated.
2. The sub-element cross-section is, automatically dependent on the cross-section, divided into sub-areas and the axial and shear stress is calculated for each sub-area as shown below for wide flange and tubular cross-sections. Other cross-sections are similar.

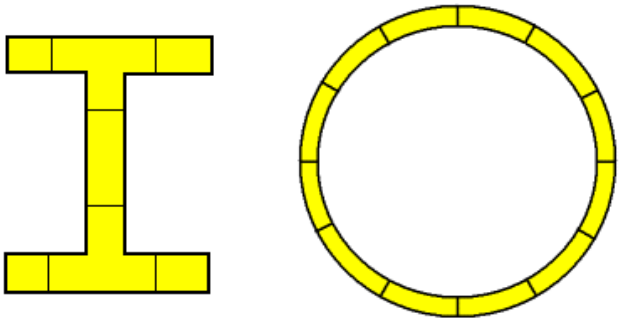

FIGURE A.2: Wide flange and tube division. [2]

3. For each sub-area, the plasticity is determined by calculating the amount of strain which exceeds the von Mises-Hencky stress envelope. The plastic strain is retained for each sub-area of each sub-element through out the loading sequence to facilitate the unloading of a sub-area if required.

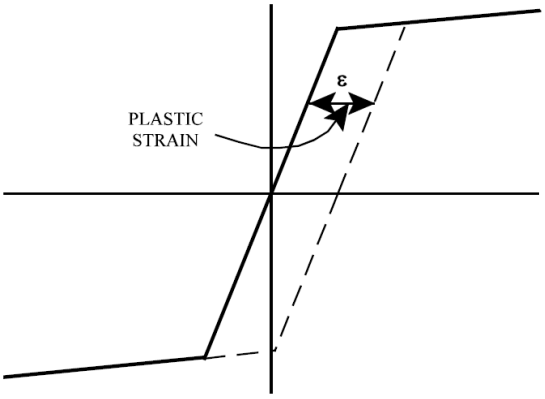

FIGURE A.3: Plastic strain. [2]

4. If the local buckling is to be included, the strain is compared to the local buckling strain level of the following:

$$\varepsilon_{lb} = \frac{16}{\left(\frac{D}{t}\right)^2} \tag{A.30}$$

   If this value is exceeded, a hinge is formed and the sub-element will have zero moment capacity.

5. The plastic stresses are then used to compute self-equilibrating plastic forces on each sub-element.

6. These plastic forces are then used in the member iterative solution.

7. After the final member iteration, the resulting end plastic forces are transformed into the global coordinates and added to the global plastic force vector.

8. The final member stiffness is calculated on the final deflected position of the sub-elements.

Appendix B

Basic equation for beams

The derivation of the Euler-Bernoulli beam theory will be given in this appendix by following the approach of [12]. The relation for an elastic perfect plastic material (figure 3.1b) with a symmetric shaped plate girder with pure bending loading Q will be derived. It is assumed that the beam element is in an unloaded state and it is free of stresses and curvatures. Also the beam is considered to be long compared to the width and depth. This means that the lateral, or transverse, shear stresses are small compared with the axial, or longitudinal, stresses. These assumptions simplify the analyses for elastic beams, but these assumptions are also acceptable for the behaviour of perfectly plastic beams.

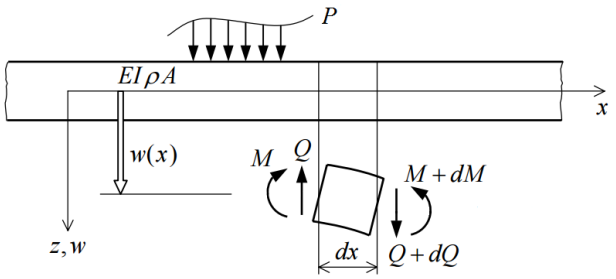

FIGURE B.1: Sign convention for prismatic Euler Bernoulli beam.[12]

The relation between moments and curvatures can be derived as follows:

The kinematic equation is described as

$$\varepsilon(z) = \kappa\, z \tag{B.1}$$

where

$$\phi = -\frac{dw}{dx}; \quad and \quad \kappa = \frac{d\phi}{dx} = -\frac{d^2w}{dx^2} \tag{B.2}$$

The Hooke's law describes the constitutive equation as

$$\sigma(z) = E\,\varepsilon(z) \tag{B.3}$$

this produces a linear stress function across the height of the beam $\sigma(z) = z\,E\,\kappa$ and thus the bending moment becomes

$$M(x) = \int_A z\sigma(z)dA = E\,\kappa \int_A z^2 dA \rightarrow M = EI\,\kappa \tag{B.4}$$

where

$$I = \int_A z^2 dA \tag{B.5}$$

Newton's second law describes that the moment and lateral force equilibrium equations for the beam in figure B.1 as

$$\frac{dM}{dx} = Q \tag{B.6}$$

and

$$\frac{dQ}{dx} = -P \tag{B.7}$$

Knowing the relation between curvature and moment written in equation B.4 and differentiating equation B.6 to x and substituting it to equation B.7 the governing static equation for the beam displacement can be written as:

$$EI\frac{d^4w}{dx^4} = P \tag{B.8}$$

Appendix C

Results SACS plastic analysis

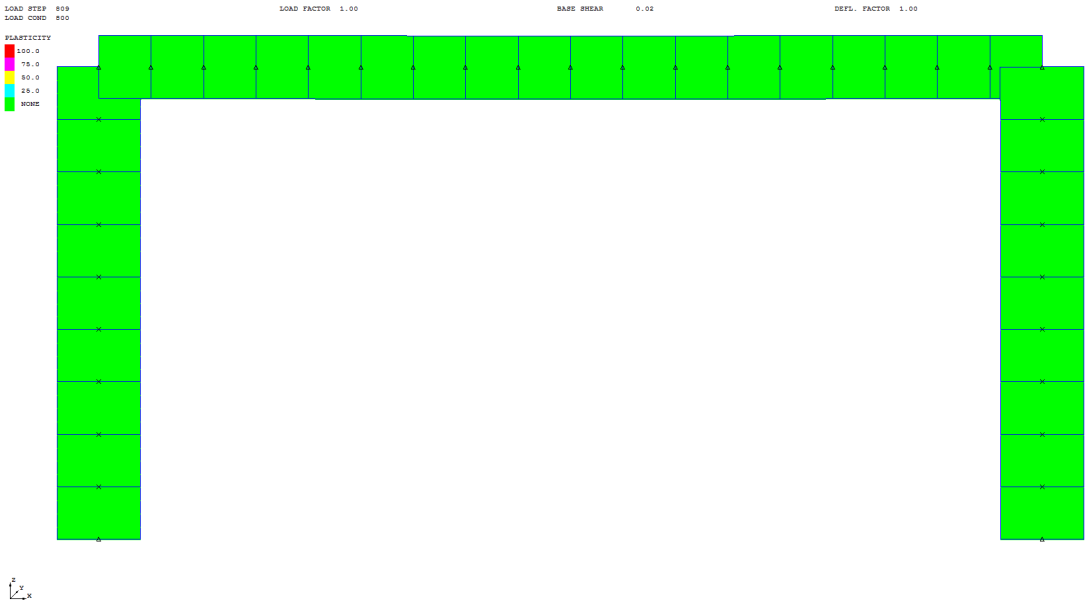

FIGURE C.1: Case1

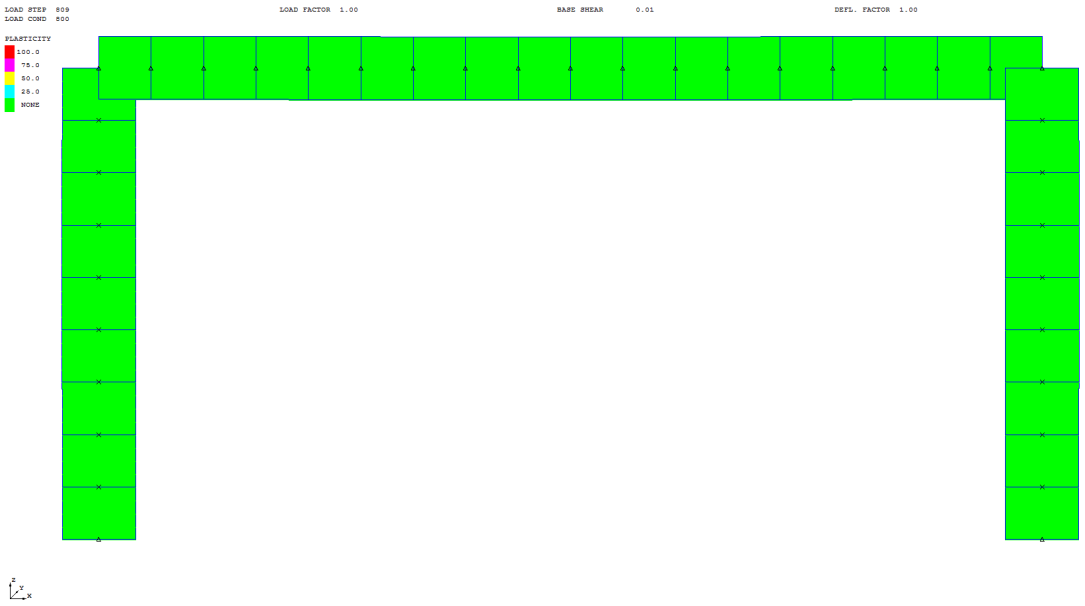

FIGURE C.2: Case2

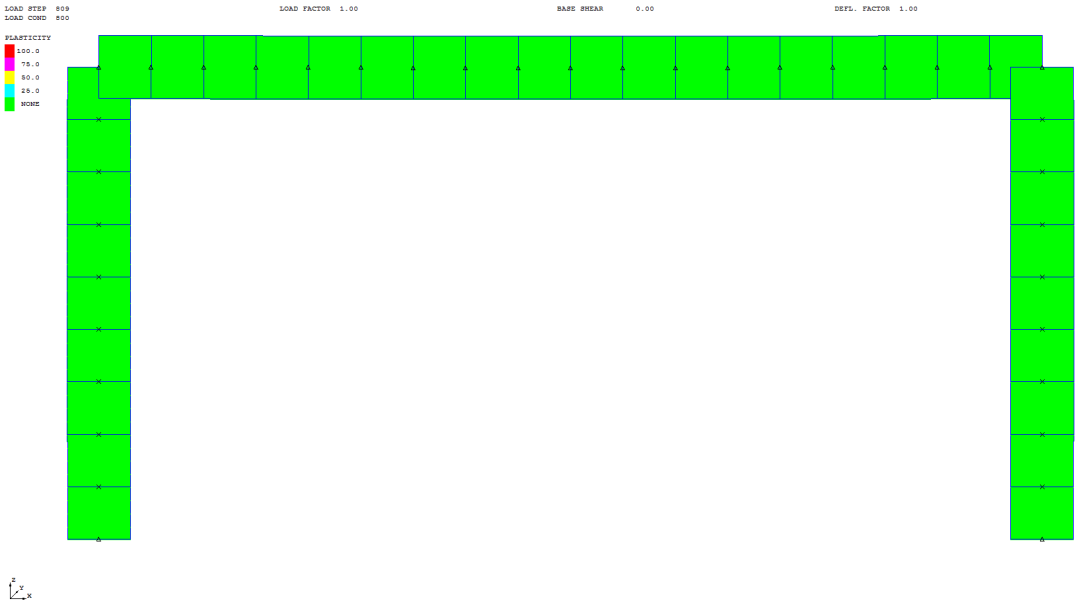

FIGURE C.3: Case3

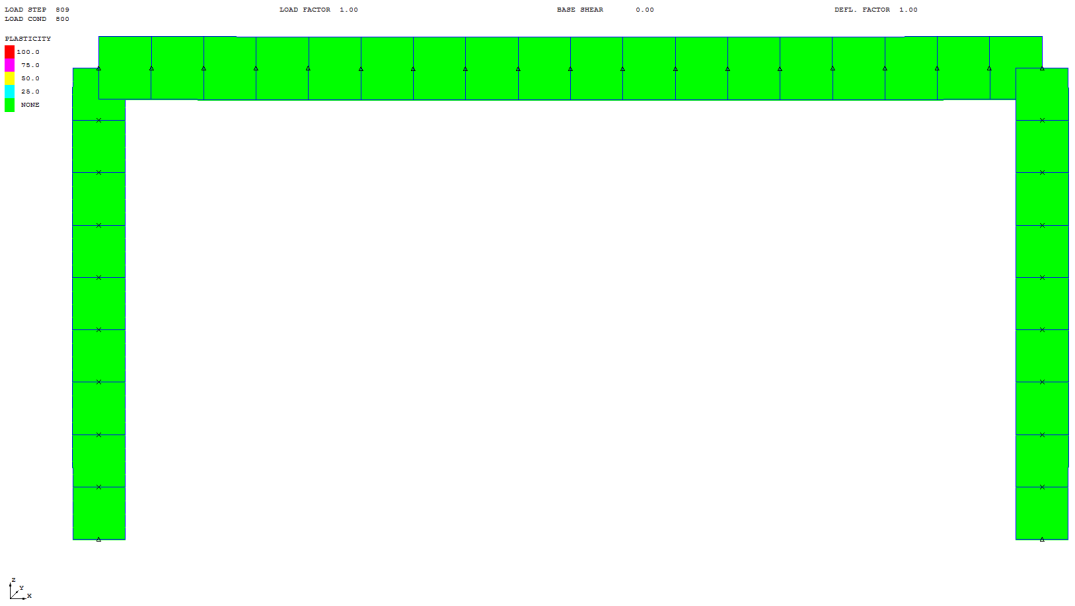

FIGURE C.4: Case4

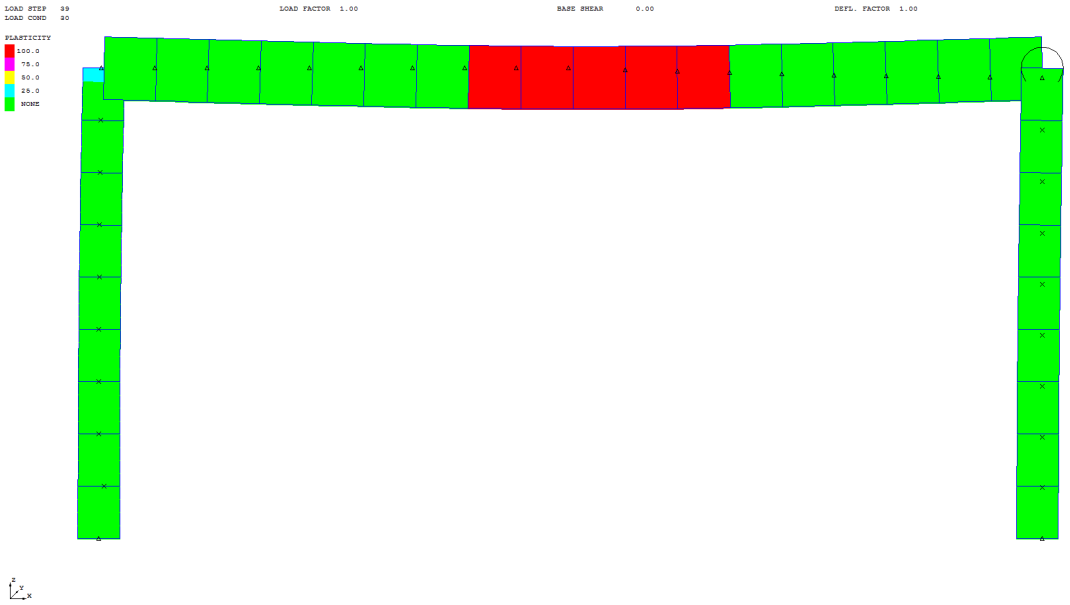

FIGURE C.5: Case5

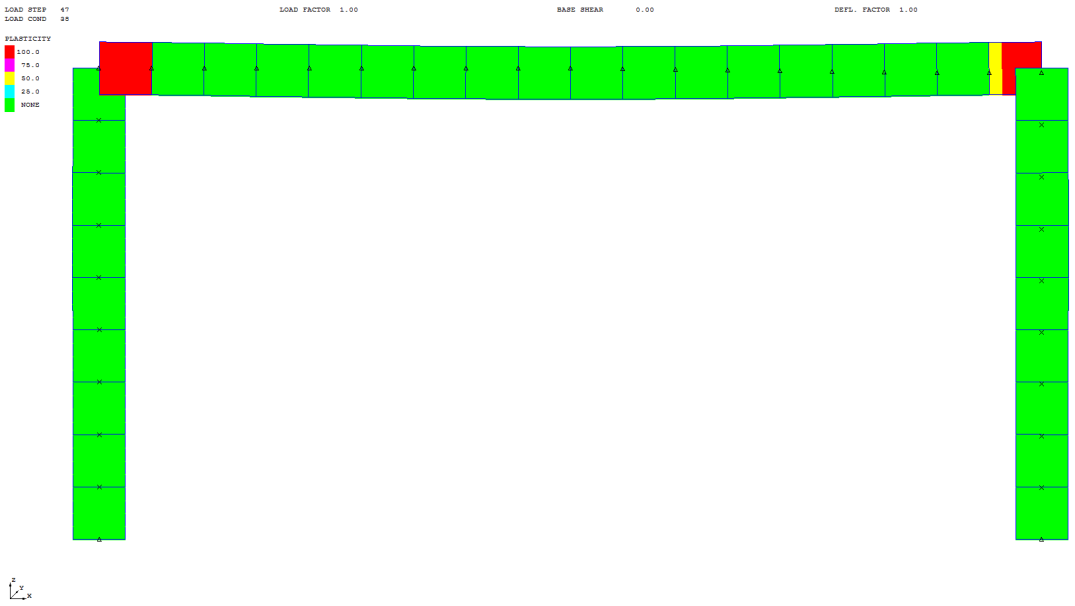

FIGURE C.6: Case6

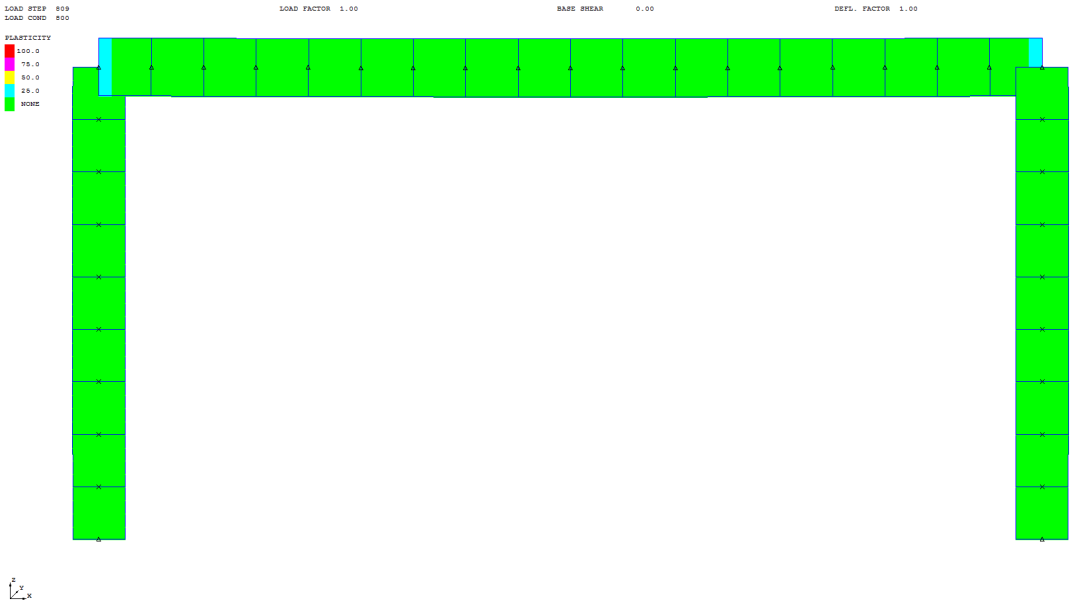

FIGURE C.7: Case7

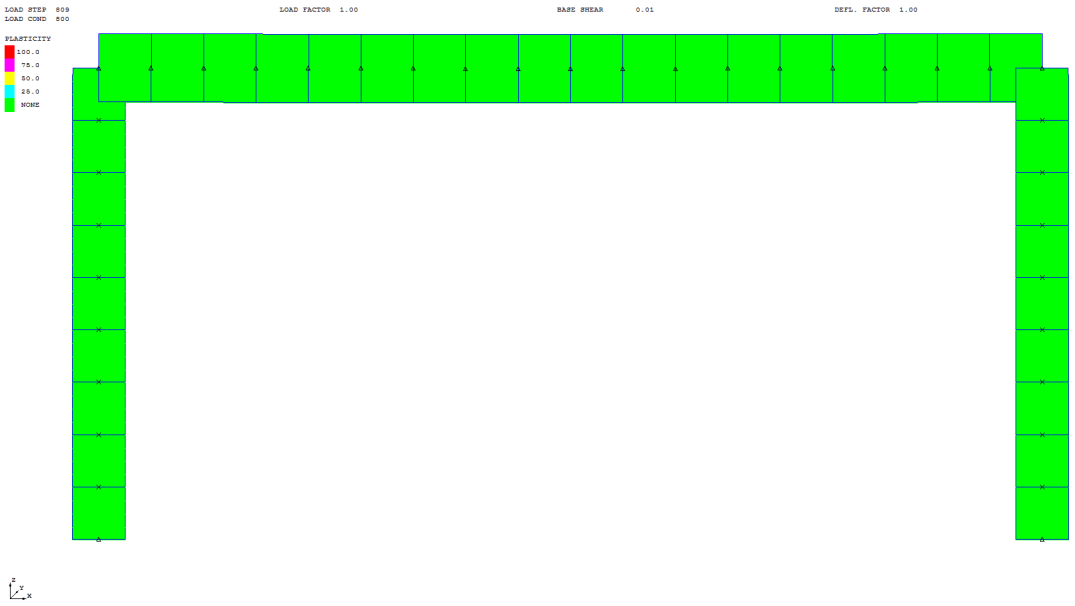

FIGURE C.8: Case8

Appendix D

Frame formula

The bending moments of the statically indeterminate frame of figure D.1 will be calculated with the help of the basic equations of beam deflection. This structure had no moveable nodes.

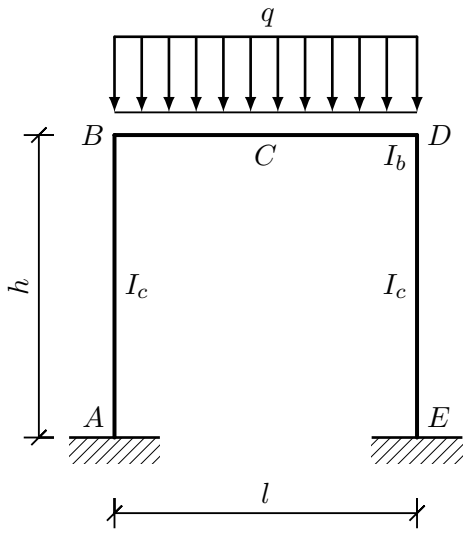

FIGURE D.1: Example frame

The structure is divided in parts to solve the unknown moments with the use of standard load types.

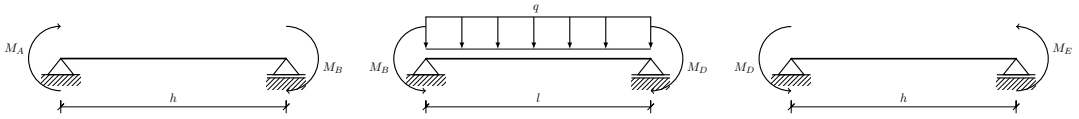

FIGURE D.2: Frame split in parts

Due to the symmetry only two unknown moment M_A and M_B have to be find. The following conditions have to be met:

$$\varphi_B^{(AB)} = \varphi_B^{(BD)} \tag{D.1}$$

and

$$\varphi_A = 0 \tag{D.2}$$

With use of the rotation and displacement relations (also known as the forget-me-nots) the equation of D.1 becomes:

$$-\frac{M_B \cdot h}{3EI_c} + \frac{M_A \cdot h}{6EI_c} = -\frac{q \cdot l^3}{24EI_b} + \frac{M_B \cdot l}{3EI_b} + \frac{M_D \cdot l}{6EI_b} \tag{D.3}$$

and D.2 yields:

$$-\frac{M_A \cdot h}{3EI_c} + \frac{M_B \cdot h}{6EI_c} = 0 \Rightarrow M_A = \frac{1}{2}M_b \tag{D.4}$$

Due to the symmetry $M_A = M_E$ and $M_B = M_D$, this gives:

$$-\frac{M_B \cdot h}{3EI_c} + \frac{M_B \cdot h}{12EI_c} = -\frac{q \cdot l^3}{24EI_b} + \frac{M_B \cdot l}{3EI_b} + \frac{M_B \cdot l}{6EI_b} \tag{D.5}$$

simplifying the equation gives:

$$M_B \cdot \left(\frac{h}{4I_c} + \frac{l}{2I_b}\right) = \frac{q \cdot l^3}{24I_b} \tag{D.6}$$

After rearranging, the equation becomes:

$$M_B = \frac{q \cdot l^3}{6I_b \cdot \left(\frac{h}{I_c} + \frac{2l}{I_b}\right)} \tag{D.7}$$

Introducing ratios for the length and height of the beam $\alpha = \frac{h}{l}$ and the area moment of inertia of the beam and column $\beta = \frac{I_b}{I_c}$ the equation of D.7 becomes:

$$M_B = \frac{q \cdot l^2}{6(\alpha\beta + 2)} \tag{D.8}$$

Now the other moments in the frame can be written:

$$M_D = \frac{q \cdot l^2}{6(\alpha\beta + 2)} \tag{D.9}$$

$$M_A = M_E = \frac{q \cdot l^2}{12(\alpha\beta + 2)} \tag{D.10}$$

The moment in the middle of the beam M_C can be described as:

$$M_C = M_B - \frac{q \cdot l^2}{8} = \frac{q \cdot l^2}{6(\alpha\beta + 2)} - \frac{q \cdot l^2(\alpha\beta + 2)}{8(\alpha\beta + 2)} = -\frac{q \cdot l^2(3\alpha\beta + 2)}{24(\alpha\beta + 2)} \tag{D.11}$$

It is interesting to find the values of α and β where the moments in location B and C are the same in magnitude, but obviously different in sign (so ignoring the sign difference).

$$M_B = M_C = \frac{q \cdot l^2}{6(\alpha\beta + 2)} = \frac{q \cdot l^2(3\alpha\beta + 2)}{24(\alpha\beta + 2)} \Rightarrow \frac{1}{6} = \frac{3\alpha\beta + 2}{24} \tag{D.12}$$

This leads to:

$$\frac{2}{3} = \alpha\beta = \frac{h}{l} \cdot \frac{I_b}{I_c} \tag{D.13}$$

So, when the product of the ratios is equal to $\frac{2}{3}$ the bending moments at the end side of the beam and midspan of the beam are equal. This shows also that the ratios, α and β have the same influence regarding redistribution by reducing/increasing moments in the midspan or at the side of the beam. In other words the same results could be achieved when e.g. instead of increasing the stiffness of a beam the length of the beam could be decreased. However it is more efficient to change the moment of inertia of the beam or column, because a relative small change on height of the beam has a larger impact on the inertia. Furthermore, when $\alpha\beta < \frac{2}{3}$ then the moments at the sides of the beam will be larger than the midspan and when $\alpha\beta > \frac{2}{3}$ then the moment at the midspan will be larger than the moments at the sides of the beam.